

Towards an understanding of the carbon isotopic changes across the Toarcian oceanic anoxic event

by

Alison Margaret Cohen

Submitted to the Department of Earth, Atmospheric and Planetary Sciences

in partial fulfillment of the requirements for the degree of

Master of Science

at the

MASSACHUSETTS INSTITUTE OF TECHNOLOGY

September 2005

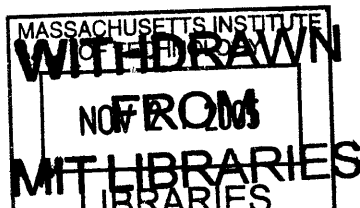
© Massachusetts Institute of Technology 2005. All rights reserved.

Author
Department of Earth, Atmospheric and Planetary Sciences
August 25, 2005

Certified by
Daniel H. Rothman
Professor
Thesis Supervisor

Certified by
Roger E. Summons
Professor
Thesis Supervisor

Accepted by
Maria T. Zuber
Chairman, Department of Earth, Atmospheric and Planetary Sciences



LINDGREN

Towards an understanding of the carbon isotopic changes across the Toarcian oceanic anoxic event

by

Alison Margaret Cohen

Submitted to the Department of Earth, Atmospheric and Planetary Sciences
on August 25, 2005, in partial fulfillment of the
requirements for the degree of
Master of Science

Abstract

A combination of bulk carbon, biomarker and compound specific isotopic analyses were used in order to investigate the changes which accompanied the deposition of black shales during the upper *tenuicostatum* and lower *falciferum* zones of the Toarcian (early Jurassic, 183 Ma) ocean anoxic event (OAE).

In this study, we reveal that apparent negative isotopic excursions in bulk organic and carbonate carbon were the result of compositional changes of organic matter and diagenesis, respectively. Organic petrology and Rock-Eval pyrolysis of organic matter from the Jet Rock, Hawsker Bottoms, Yorkshire, England, show that the upper *tenuicostatum* zone contains very large amounts of terrigenous debris. A careful review of the carbonate carbon record, as reported in the literature, indicates that a large negative isotopic excursion in bulk carbonate is likely the result of diagenesis, rather than reflective of seawater isotopic conditions.

Biomarker distributions and isotopic composition of primary production biomarkers show little variation during the largest changes in the bulk records. Biomarker source indicators vary little throughout the section, indicating little change in biota or redox structure of the water column during this widespread deposition of black shales. Isotopic compositions of algal short chain *n*-alkanes, pristane and phytane also remain steady across the section. Long chain *n*-alkanes, biomarkers for higher plants, also do not change during the event. Isorenieratane, a biomarker for green sulphur bacteria and an indicator of photic zone euxinia, however, show a strong peak in concentration coincident with the maximum abundance of organic carbon.

Because we have found no evidence for significant isotopic variation on land or in the ocean, we must infer that there were no major redistributions of carbon in the ocean-atmosphere system during the Toarcian OAE. Therefore, oceanic overturn or large input of methane are not plausible explanations for this event. This deposition of black shales was a result of periodic episodic euxinia, which resulted in the increased preservation of organic matter. We believe that this event was not a large, one-time occurrence, but a characteristic response to paleogeography and oceanic circulation patterns of the Mesozoic.

Thesis Supervisor: Daniel H. Rothman
Title: Professor

Thesis Supervisor: Roger E. Summons
Title: Professor

Acknowledgments

I would like to thank Professor Darren Gröcke for providing samples, as well as meaningful discussion about and insight on the Toarcian OAE. I would also like to thank Professor Martin Jones at University of Newcastle for carrying out the Rock-Eval pyrolysis, Dr. Lorraine Eglinton at W.H.O.I. for her expert work in organic petrology, Dr. Emmanuelle Grosjean at M.I.T. for help in biomarker preparation and analysis, and Sean Sylva at W.H.O.I. for his help and expertise with the Delta IRMS system. Finally, I'd like to thank the M.I.T. Geobiology lab, and especially Professors Daniel Rothman, Roger Summons and John Hayes for dedicating their time and resources to me.

Contents

1	Introduction	13
1.1	Background	14
1.2	Materials and methods	16
1.2.1	Samples	16
1.2.2	Experimental methods	16
2	Bulk carbon records	19
2.1	Results from bulk organic carbon analyses	19
2.1.1	Rock-Eval pyrolysis and bulk organic carbon isotopes	19
2.1.2	Organic petrology	20
2.2	Marine carbonate isotopic record	21
3	Biomarker ratios	25
3.1	Organic matter maturity	25
3.2	<i>N</i> -alkane and isoprenoid distributions	26
3.3	Source indicators	26
3.4	Isorenieratane	27
4	Compound-specific isotope analysis (CSIA)	29
4.1	Results of CSIA analyses	29
4.2	Chromatography of desulfurized samples	30
4.3	The isotopic composition of terrestrial organic matter	31

5 Discussion	33
5.1 Estimate of δ_m , the isotopic composition of marine organic carbon . .	33
5.2 Periodic euxinia	35
5.3 Implications for the methane hypotheses	37
6 Conclusion	39
A Abbreviations	41
B Definitions of biomarker ratios	43
C Tables	45
D Figures	47

List of Figures

D-1	Bulk data from the Hawsker Bottoms section of the Toarcian black shale deposition. Section is thought to last 500-700 k.y. [18, 1]. (a) Percent total organic carbon, (b) isotopic composition of total organic carbon, δ_{toc} , (c) $\delta_{\text{belemnites}}$, isotopic composition of belemnite fossils, (d) hydrogen index (HI), and (e) percent of bulk composition that is terrigenous matter as determined through organic petrology. Chemostratigraphy as shown in Refs. [28] and [21]. $\delta_{\text{belemnites}}$ data from Ref. [28].	48
D-2	Marine and terrigenous microfossils from the Jet Rock, Hawsker Bottoms, Yorkshire, England from kerogen isolates. Scale bars are $50\mu\text{m}$. (a) and (b) Comparison of marine (25% terrigenous) and woody (80% terrigenous) end members under transmitted light; and (c) and (d) in fluorescing light.	49
D-3	Estimate of δ_{m} , the isotopic composition of marine organic carbon, using Equation (5.2) and different assumptions for the isotopic composition of terrestrial material, δ_{t} . Light grey lines are δ_{toc} and δ_{t} . δ_{t} data is from Hesselbo (2000) [16].	50
D-4	Distribution of hopanes and other pentacyclic triterpanes in the saturated fraction of sample ENR004, at height +5.9 m. Data was obtained by GC-MS MRM transitions $\text{M}^+ \rightarrow 191$. Compounds are identified by carbon number and relative elution times. For abbreviation definitions, see Appendix A.	51

D-5	Distribution of steranes in the saturated fraction of sample ENR004, at height +5.9 m. Data was obtained by GC-MS MRM transitions $M^+ \rightarrow 217$. Compounds are identified by carbon number and relative elution times. For abbreviation definitions, see Appendix A.	52
D-6	Distribution of methylhopanes in the saturated fraction of sample ENR004, at height +5.9 m. Data was obtained by GC-MS MRM transitions 426 \rightarrow 205. Compounds are identified by carbon number and relative elution times. For abbreviation definitions, see Appendix A.	53
D-7	Selected saturate fraction distributions through the section. Labelled peaks are (a) $n-C_{17}$ (b) pristane (c) $n-C_{18}$ and (d) phytane, along with $n-C_{25}$ through $n-C_{31}$	54
D-8	Ratios of selected source biomarkers across the section. Calculations of biomarker parameters are found in Appendix B.	55
D-9	Identification of isorenieratane, a biomarker for green sulphur bacteria, in sample ENR005, at height +6.9 m.	56
D-10	Isorenieratane concentration normalized to total organic carbon abundance.	57
D-11	$\delta^{13}C$ of $n-C_{17}$, $n-C_{18}$, pristane and phytane across the section.	58
D-12	Saturated fraction of desulfurized hydrocarbons, from sample ENR001 at +3.2 m.	59
D-13	$\delta^{13}C$ of all the n -alkanes of selected samples.	59
D-14	Variation of the isotopic composition of short chain ($n-C_{17}$ to $n-C_{19}$) and long chain ($n-C_{27}$ to $n-C_{31}$) through the oceanic anoxic event.	60
D-15	Best estimates of δ_m , total marine organic carbon and the error ascribed to it, δ_t bulk terrestrial organic carbon, δ_{carb} marine carbonate and ϵ through the Hawsker Bottoms section. Calculations and assumptions are described in Section 5.1. δ_{carb} from McArthur (2000) [28].	61

List of Tables

A.1	Abbreviation for compounds identified in Figures D-4 and D-5.	42
B.1	Calculation of biomarker ratios shown in Table C.2 and Figure D-8. .	43
C.1	Bulk geochemical data for the sample suite.	45
C.2	Biomarker ratios and compound-specific isotope data for sample suite (shown in stratigraphic order from lowest to highest. For parameter definitions and ratio calculations, see Appendix B).	46

Chapter 1

Introduction

Widespread deposition of organic-rich rocks, known as black shales, over specific time intervals has long received much attention in the geologic community. When such a deposition is accompanied by a global increase in the abundance of ^{13}C in carbonate carbon, these time periods have been named ‘Ocean Anoxic Events’ (OAE’s) [42]. Originally, several such periods were recognized in the Cretaceous.

Jenkyns (1988) [18] recognized global deposits of black shales and a positive isotopic excursion in carbonate carbon in Tethyan Europe during the Toarcian period of the early Jurassic (183 Ma), leading to its classification as an OAE. Subsequent work on this event, however, revealed that its geochemical signature is not so straightforward. Carbonate records show both negative and positive excursions in the abundance of ^{13}C , while the organic carbon record demonstrates a 6‰ negative excursion. The conflicting carbonate signals and the large and rapid nature of the organic carbon excursion have caused much speculation as to the causes, consequences and extent of this event.

A combination of bulk-rock analysis coupled with biomarker and compound-specific isotope analysis of organic matter has yielded insight into changes which occurred during several environmental and evolutionary events in earth history (e.g. [14, 13]) and which bulk organic matter analyses alone could not reveal. Here, such a multi-faceted approach is undertaken in order to better understand the biogeochemical processes which occurred during the deposition of black shales in the Toarcian

period.

First, bulk composition data is presented which reveals that just before the peak of the black shale deposition, the organic matter contains a large terrigenous component. Then, the carbonate carbon record is investigated in detail in attempt to determine the true, oceanic isotopic signal of carbonate carbon. Biomarker ratios and compound-specific isotope data from samples spanning the event are presented. Best estimates are made for the isotopic composition of terrestrial organic carbon, marine organic matter and marine carbonate across the Toarcian OAE.

1.1 Background

Early Jurassic paleogeography and environment were fundamentally different from the modern world. The Tethys Ocean, enclosed on the north and south by a single, arid supercontinent, Pangaea, touched the global ocean to the east. The west side of this ocean bordered what is now northern Europe. The region had broad, shallow epicontinental seas containing numerous small islands. This area was newly open to the Arctic Ocean via the Viking Straits [3]. Temperatures are thought to have been 5-10°C warmer than today [1], with a vast amount of land at low latitudes and probable temperate high latitudes [1]. The average isotopic composition of carbonate carbon deposited from the oceans was +2‰, compared to 0‰ today [48]. Organic carbon was significantly depleted in ^{13}C , averaging -30‰, compared to -22‰ today [15]. Thus, the average fractionation between inorganic and organic carbon, known as ϵ_{toc} , was a staggering 32‰ (compared to 25‰ today).

This black shale event, which endured 500 to 700 k.y. [18, 1, 28], witnessed significant volatility in the environment and the biota. The rift between North America and Europe/Asia had begun to form the proto-Atlantic Ocean. The Karoo-Ferrar flood basalt province is dated to this very time, 183 ± 2 m.y., indicating major volcanism in southern Africa, possibly related to the breakup of the continent [32]. In this short interval of time, sea level rose 10-50 m [12], temperature warmed about 6-7°C [1, 38], and a mass extinction affected benthic fauna [25].

Black shales were deposited most intensely in northern Europe. The Toarcian OAE includes extremely organic-rich deposits in famous sections in England, Germany and France, known as the Jet Rock, Posidonienschiefer and Schistes Carton, respectively. In contrast, Tethyan sections at open-ocean settings, show lower abundances of organic matter [18, 19].

Several different hypotheses have been posed to explain the geological and geochemical signals in sections which include this event. The deposition of black shales was originally thought to stem from increased productivity sparked by sea-level rise across the *falciferum* zone, causing increased burial of organic carbon and a positive excursion in the ^{13}C abundance of carbonate carbon [18, 19]. Other studies, which found coinciding negative excursions in carbonate and organic carbon, concluded that the event stemmed from density stratification, which was followed by basin stagnation, recycling and upwelling of bottom waters rich in isotopically depleted CO_2 , causing negative excursions in both global reservoirs [24, 40, 43]. The most well-known recent hypothesis holds that very large amounts of carbon from methane hydrates entered the oceanic and atmospheric carbon reservoirs, causing coincident negative excursions in the isotopic composition of fossil wood and bulk organic carbon through the Jet Rock section [16, 2]. Most recently, however, a new study has retreated from the methane-hydrate hypothesis but poses that magmatic intrusions in southern Pangaea caused the release of large amounts of thermogenic methane, ultimately leading to the OAE [29].

Because these theories pose widely divergent causes and consequences, the bulk and compound-specific properties of the organic matter during the Toarcian black shale deposition were studied in order to narrow the range of possible interpretations of geochemical signals during this event.

1.2 Materials and methods

1.2.1 Samples

Samples for the current study come from the outcrops of Jet Rock at Hawsker Bottoms, Yorkshire, England, which was located in the northern European epicontinental seas described above. They are a subset of the samples used in Ref. [21]. The samples are carbon-rich, millimeter-laminated black shales with intercalated layers of calcite concretions. The thickness of section is 14 m, with sampling approximately every meter. The Jet Rock section yields a high-resolution dataset across the black shale deposition. As a result, however, a longer-term view of the entry into and recovery from the event is sacrificed.

1.2.2 Experimental methods

Rock-Eval pyrolysis

1 g aliquots of crushed sample were sent to University of Newcastle for Rock-Eval pyrolysis. This analysis ascertains the temperature of maximum hydrocarbon (HC) generation T_{\max} , which indicates the degree of thermal maturity of the kerogen. In addition, the HC generation potential, or the hydrogen index (HI), and the abundance of organic matter (TOC%) help chemically characterize the organic matter. Standard notations are used: S_1 and S_2 are in mg of hydrocarbons (HC) per gram of dry sediment and T_{\max} is expressed in °C. The hydrogen index ($HI = S_2/TOC \times 100$) is expressed in mg HC per 100 grams of TOC.

Bulk isotope analysis

Bulk sediment samples were powdered, then acidified in 37% HCl overnight at room temperature. Samples were rinsed with deionized water and centrifuged and rinsed again, until neutrality was reached. They were dried at 100°C and then weighed into tinfoil cups. Each sample was run in triplicate, so that 0.1, 0.2 and 0.5 mg of organic carbon was analysed using a Carlo Erba Elemental Analyzer connected to a Thermo-Finnigan Delta plus XP Isotope Ratio Mass Spectrometer. Standards of known isotopic composition were interspersed with samples in order to check results. Isotopic compositions are expressed relative to the Vienna PDB standard.

Biomarker analysis

Approximately 5 g of sample were used for biomarker analysis. Bitumen was extracted from the powdered samples in a Dionex ASE 200 Accelerated Solvent Extractor using a mixture of 9:1 methanol:dichloromethane at 1000 psi and 100°C. Asphaltenes were precipitated from the bitumen using *n*-pentane. Approximately 10 mg of the remaining maltene fractions were separated over a column of silica into their saturated, aromatic and polar fractions using respectively hexane, hexane / dichloromethane (DCM) 1:1 (v/v) and DCM / methanol 7:3 (v/v) as eluents.

n-Alkanes were separated from the non-linear saturated hydrocarbons using 5 angstrom molecular sieve. Activated molecular sieves were added to the saturated hydrocarbon fractions dissolved in cyclohexane in a sealed reactive jar and heated at 80°C overnight. The molecular-sieve non-adduct (MSNA) fraction was removed and prepared for GC-MS analysis. *n*-Alkanes were retrieved from the molecular sieve by dissolving the pellets in hydrofluoric acid, subsequently extracted with pentane, and prepared for GCMS analysis.

Extracted compounds were analyzed by gas chromatography - mass spectrometry system composed of an Agilent 6890 gas chromatograph with an Agilent 5973 mass spectrometer. The saturated hydrocarbon samples were diluted to 1 mg/100 μ L in hexane and transferred to a GC vial. Injections were made using an HP6890 autosampler. The column was a 60 m Chrompack CP8744 CPsil-5CB with an internal diameter of 0.32 mm, film thickness of 0.25 μ m. The carrier gas was helium of a volumetric flow rate of 1.6 mL/min. The ion source temperature of the was 250°C source temperature. Samples were analyzed using both full scans and selected-ion monitoring methods for a more detailed analysis of specific compounds. Aromatic fractions were spiked with 414 ng of D₁₄ - *p*-terphenyl standard to facilitate quantification of aromatic hydrocarbons such as isorenieratane.

Gas chromatography coupled to tandem mass spectrometry used a Hewlett-Packard 6890 gas chromatograph coupled to a Micromass Autospec Ultima operated in the metastable-reaction-monitoring (MRM) mode. A 60-m J&W Scientific DB-1 fused silica capillary column (0.25 mm i.d., 0.25 m film thickness) was used with helium as carrier gas. Samples were injected in pulsed splitless mode. The column temperature was programmed from 60°C (held for 2 min) to 150°C at 10°C/min, then at 3°C/min to 315°C and held isothermal for 24 min. The source was operated in EI mode at 250°C, 70 eV ionization energy and 8000 kV acceleration voltage.

Peaks were identified using previously published elution times and mass spectra. Isorenieratane peaks were identified by comparison of elution time with an authentic standard, as well as previously published mass spectra.

Compound-specific isotope analysis

n-Alkane and MSNA fractions separated for biomarker analysis were also used for compound-specific isotope analysis.

Isotope ratios were measured using gas chromatography - isotope ratio mass spectrometry (GC-IRMS) on a Finnigan MAT Delta Plus XL coupled to an Agilent 6890

GC via the Finnigan GCC III combustion interface. The column was a 30 m DB-5MS 320 μ m ID with a 0.25 μ m film thickness. $\delta^{13}\text{C}$ values (versus PDB) were calculated by integrating the mass 44, 45 and 46 ion currents of the CO_2 peaks produced by combustion of the column effluent and those of either CO_2 spikes or an internal standard of a known $\delta^{13}\text{C}$ value. Accuracy was checked using an internal standard of a known isotopic composition.

Raney nickel desulfurization

Polar fractions from four representative samples were selected (at heights -2.7 m, 0.6 m, +3.2 m and +6.1 m) for Raney nickel desulfurization in order to liberate and analyze GC-amenable hydrocarbons linked to geomacromolecules by sulfur bonds. 10-30 mg of sample, combined with Raney nickel suspended in ethanol and toluene, was brought to reflux for three hours under argon. After work up, the resulting hydrocarbons were separated on a silica gel column into saturated, aromatic and polar fractions. The hydrocarbons contained in the saturated fractions were then further analyzed using GC-MS.

Organic petrology

Four representative samples (at heights -3.4 m, +0.3 m, +3.2 m and +5.1 m) were chosen for studies of the organic petrology. Standard procedures were followed for isolation of kerogen from 3 - 4 g aliquots of extracted rock. Samples were treated overnight once with hydrochloric acid (HCl), twice with hydrofluoric acid (HF) and once more with HCl. In between treatments, samples were centrifuged and rinsed. Prior to analysis, samples rinsed three times with water and twice with methanol.

A sub-aliquot of homogenized dry kerogen was suspended in methanol and then mounted onto a glass slide using mounting medium, and set at room temperature. Duplicate slides were prepared for each sample. Samples were examined using a Zeiss research microscope in white light and fluorescent light using a Zeiss x 40 Plan-Neofluar objective. Photomicrographs were taken using a Zeiss Axioskop and Axio Image D1. Fluorescence images were obtained using a Zeiss 18 filter set.

Chapter 2

Bulk carbon records

New data from Rock-Eval pyrolysis and organic petrology are used to elucidate the different sources of the bulk organic matter. Then, a detailed literature review of the carbonate carbon isotopic record is undertaken in attempt to recognize the authentic marine signals in this record.

2.1 Results from bulk organic carbon analyses

2.1.1 Rock-Eval pyrolysis and bulk organic carbon isotopes

Table C.1 and Figure D-1 reveal changes in the bulk composition of the rocks as the Toarcian OAE was traversed. The whole section is characterized by levels of total organic carbon (TOC%) greater than 2%. Abundances gradually increase to a maximum of 11% at height +3.2 m in the middle *exaratum* subzone before dropping back to 5% at the top of the section.

The isotopic composition of bulk organic carbon, δ_{toc} , shows a 7‰ negative excursion, beginning at -25‰ in the *tenuicostatum* zone. It drops to -32‰ before recovering to -27‰ in the upper *exaratum* subzone. The bulk organic carbon isotopic composition is strongly negatively correlated to TOC% ($r = 0.85$).

Hydrogen index (HI) values range from 200 mg/g TOC in the *tenuicostatum* zone to a maximum of 440. Generally, marine algal organic matter has high HI values,

whereas lower values indicate the presence of plant material, with low hydrocarbon yields. The hydrogen index has a significant positive correlation with TOC% ($r = 0.68$), and negative correlation with δ_{toc} ($r = 0.67$)¹.

The relationship between HI and TOC% indicates that as the amount of organic matter increases, it tends to be more lipid-rich, and thus more marine-sourced. In addition, the more marine-sourced the organic matter, the more depleted it is isotopically. These relationships were noted in Cretaceous black shales in Dean (1986) [8], and attributed to a decreasing terrestrial input in the more depleted and more hydrocarbon-rich organic carbon.

2.1.2 Organic petrology

To assess the amount of terrigenous input in the kerogen, four samples were chosen for organic petrological analysis. Results, shown in Figure D-1(e), indicate that the *tenuicostatum* zone sample at -3.4 m is made up of 80% terrigenous matter. Microscopic analysis reveals that this terrigenous matter consists of mostly inertinite and vitrinite, as shown in Figure D-2(a) and (c). In contrast, the analyzed samples in which organic carbon was most depleted in ¹³C (at +0.3 m and +3.2 m) are the richest in amorphous algal organic matter, implying a marine source, as shown in Figure D-2(b) and (d). These results agree with the conclusions from the Rock-Eval pyrolysis, discussed above.

It appears that this terrigenous matter is not simply a local phenomenon in the Hawsker Bottoms section, but is prevalent throughout the European Toarcian black shales. The four studies which have reported hydrogen index values show low values for the upper *tenuicostatum* zone (Germany [43, 36], Italy [10], England [47]), though none discussed the possibility of terrigenous input.

¹Excluding the sample at -2.7 m which has an anomalously high HI value, $r = 0.79$ and $r = 0.84$ for δ_{toc} vs. HI and TOC% vs. HI, respectively.

2.2 Marine carbonate isotopic record

The Toarcian OAE was originally identified in Jenkyns and Clayton (1986) [19] and Jenkyns (1988) [18] by widespread black shale deposition accompanied by a positive excursion in δ_{carb} . Although these original studies of the bulk carbonate of seven Tethyan sections showed some negative excursions in bulk δ_{carb} , detailed examination of these samples found $\delta^{18}\text{O}$ isotopic compositions which strongly correlated with δ_{carb} . These results, which have not since been refuted, led the authors to conclude that each of the negative excursions were caused by early diagenetic effects and that the true oceanic signal is a positive $\delta^{13}\text{C}$ excursion of 2 to 3‰ across the *exaratum* subzone.

Since this original work, numerous studies have shown both positive [39, 22, 28, 37, 20, 21, 1] and negative excursions [20, 43, 21, 36, 47] in δ_{carb} . On first appraisal, this record appears to be too inconsistent and too altered by local effects to distill any global oceanic signal from it. A closer look, however, reveals that every negative excursion reported is either (a) accompanied by evidence hinting it is most likely diagenetic, or (b) supported by no evidence at all showing it is representative of primary oceanic dissolved inorganic carbon and not a remnant of diagenesis. Here, the δ_{carb} record is examined in detail, and we conclude that the primary oceanic record is a positive excursion of 2 to 4‰ in the *exaratum* subzone of the *falciferum* zone.

The bulk carbonate record of the Mochras Farm borehole in England exhibits a sharp drop of 6‰ across the *exaratum* subzone from +2 to -4‰. This record was shown originally in Jenkyns and Clayton (1997) [20], reprinted in Jenkyns et. al. (2001) [21], and re-analyzed in van de Schootbrugge et. al. (2005) [47]. Jenkyns and Clayton (1997), the original study of this section, however, called the effects of diagenesis ‘so pervasive’, that no primary oxygen isotopes could be discerned. They conjectured that the unusually low δ_{carb} values stemmed from the input of carbonate derived from reactive organic matter during early diagenesis. Trace element compositions were not reported, and the weight percent CaCO_3 was a suspiciously low 10-20% during the negative excursion. These pieces of evidence, and the unrefuted conclu-

sions by the original authors lead us to the conclusion that the negative excursion in δ_{carb} at Mochras Borehole is likely diagenetic.

A striking example of the mistaken identification of an ‘excursion’ is demonstrated in the carbonate records of the Dötternhausern section of the German Posidonia shale, where three different studies have measured δ_{carb} . Schouten et. al. (2000) [43] and Röhl et. al. (2001) [36] found a large *negative* excursion in bulk carbonate, extending to -7 and -11‰, respectively, whereas Bailey (2003) [1], who analyzed the carbon isotopic composition of belemnite shells, found a *positive* excursion with values no lower than 0‰ [1]. Neither of the bulk carbonate datasets was accompanied by trace element analysis to assess the possible diagenetic contribution of the negative excursion. In contrast, the belemnite study confirmed that the signal is of primary origin using $\delta^{18}\text{O}$, trace element concentrations and strontium isotopes. It is apparent that the bulk carbonate record in England and Germany contains pervasive diagenetic imprint, while primary oceanic signals may still be extracted from belemnite shells.

The remaining section showing a negative excursion in bulk carbonate is Belluno Trough, near Dogna, Italy, shown in Jenkyns, et. al. (2001) [21]. The data, which show a change from +3 to -1‰, were published without other supporting information, such as oxygen isotopes or trace element analysis. Other information, however, indicate that this signal may be of primary origin. Percentages of CaCO_3 vary from 15 to 80% [10], unpublished oxygen isotopes show no correlation with δ_{carb} (D.R. Gröcke, unpubl. data), and the excursion appears to be secular. The overwhelming number of positive excursions documented, however, lead to the conclusion that this negative excursion is controlled by local, rather than regional or global effects.

Several studies have found positive isotope excursions in shells of extinct belemnite rostrae, in both Tethyan and northern European sections. Their dense, low-Mg calcitic shells, precipitated at or near isotopic equilibrium with ambient sea water, are less susceptible to diagenesis than bulk carbonate [37]. Petrographic, cathodoluminescence and geochemical evidence, along with sampling targeted at assessing the effects of inter-species and intra-sample variation give confidence that their isotopic compositions are primary. Each Toarcian study analysing belemnite shells found

a *positive* excursion, with no hint of the sudden negative drop present in the bulk carbonate record [1, 28, 39, 22, 37].

Finally, several sections for which bulk carbonate was analyzed, where the supporting evidence did not hint at diagenesis, show a positive excursion similar to that of the belemnites [18, 19].

Taking all of the above into consideration, we conclude that the primary signal which best represents conditions in the water column through the Toarcian black shales is the *positive* excursion in carbonate carbon from +2 to +5‰ across the *exaratum* subzone. The Hawsker Bottoms section exhibits a jump from +2 to +6‰ in belemnites in the upper *exaratum* subzone, as shown in Figure D-1(d) [28].

Chapter 3

Biomarker ratios

Branched alkane, aromatic and *n*-alkane fractions were separated, and analyzed using gas chromatography-mass spectrometry, as well as the highly specific metastable-reaction-monitoring-GC-MS, for quantitative biomarker analysis. Peaks were identified as shown in Figures D-4, D-5, D-6 and D-7 using published peak-identification criteria and elution times. Resulting data are shown in Table C.2.

3.1 Organic matter maturity

Biomarker ratios, shown in Table C.2, considered in concert with Rock-Eval pyrolysis data from Table C.1, reveal that organic matter in these samples is in the very early stages of oil generation. Complete hopane isomerization is indicated by the C_{31} 22S/(22S+22R) ratio of 0.59 to 0.60 for all samples, indicating that the rocks have entered the oil window [35]. Sterane isomerization, shown in the C_{29} 20S/(20S+20R) ratio, is also complete, at 0.51 to 0.53 [35]. Rock-Eval pyrolysis data, however, show that the stage of oil generation is very early, as indicated by Production Index (PI) values of greater than 0.1, but relatively low T_{max} values ($\approx 430-440^\circ\text{C}$, Table C.1). The $T_s/(T_s+T_m)$ ratios, which approach 0 prior to the oil window and 1.0 upon full maturation, range from 0.5-0.6, confirming early oil-generation maturity of the samples [35]. Finally, the methylphenanthrene index (MPI), a maturity parameter based on isomerization of specific polyaromatic hydrocarbons, yields values which are

approximately the same in all rocks, of about 0.5. Calibrations between MPI and vitrinite reflectance (R_c) yield R_c values of approximately 0.7 [4]. Similar values of R_c are calculated independently from T_{max} , confirming our assessment of the sample set at the early stage of oil generation [34].

3.2 *N*-alkane and isoprenoid distributions

The most abundant compounds in the saturated hydrocarbon fractions are *n*-alkanes, as seen in Figure D-7. The *n*-alkane distributions are generally unimodal, showing a maximum at nC_{17} and nC_{18} , extending out as far as C_{38} in some cases. Odd or even predominance of carbon numbers was not observed (carbon preference index ≈ 1 for all samples), probably a result of thermal processes [34]. Distributions of *n*-alkanes show little variability through the section.

3.3 Source indicators

Two characteristics stand out when examining the source biomarker ratio changes through the OAE, shown in Figure D-8. The most striking observation is that the ratios change little through this event which is marked so distinctly in the bulk organic carbon isotopic record. The other important observation is the extreme difference exhibited by the single sample at -4.0 m.

The biomarker ratios of this sample indicate that the organic matter derives from a very different environment from the rest of the section. A much higher pristane/phytane ratio, more C_{29} steranes, lower steranes/hopanes, gammacerane and dinosteranes all indicate that this sample comes from an oxic or terrigenous environment [34]. Its stratigraphic proximity to the nearby sample at -3.4 m, which was found to be 80% terrigenous, as discussed in Section 2.1, along with a low HI value (240 mg HC/g TOC), lead to the assessment of this sample as being dominantly terrigenous.

Biomarker ratios for the rest of the section, however, reflect a more marine en-

vironment, though not one that demonstrates a shift into and out of anoxia. The section is characterized by steady algal productivity (steranes/hopanes ratio) and salinity (gammacerane index). The 2α -methylhopane index, a well-constrained indicator of cyanobacterial input, is low (1 to 2.5%), as observed in other Phanerozoic marine black shales [45]. Its 3β isomer, which has been isolated in methanotrophs [7], appears in similar concentrations, indicated in a $2\alpha\text{MeH}/3\beta\text{MeH}$ ratio of about one throughout the section, until the uppermost sample, when 3β -MeH is more abundant. Dinosteranes, a reliable biomarker for dinoflagellates [46] with possibly some diatomic input, occur in steady amounts throughout the section, excepting the one sample at -4.0 m.

3.4 Isorenieratane

Isorenieratane is a C_{40} diaromatic carotenoid which is produced by green sulphur bacteria (Chlorobiaceae) photoautotrophic organisms which need light and H_2S . The presence of this compound in a geologic sample is a highly specific indicator for periods when euxinic conditions extended into the photic zone, indicating a very shallow oxic water column. This compound has been identified in other studies of Toarcian black shales, both in Germany and England [43, 23, 5], indicating widespread photic zone euxinia. Here, isorenieratane was identified through matching elution times with an authentic standard and published mass spectra. Figure D-9 shows the m/z 134 selected ion chromatogram of the sample at +6.9 m, along with the isorenieratane standard.

Figure D-10 shows changes in concentrations of isorenieratane normalized to total organic carbon through the section. Increasing concentrations are interpreted as increased intensity of photic zone euxinia. In contrast to the biomarker ratios, isorenieratane concentrations show significant change in the upper *exaratum* subzone, increasing to almost $1\mu\text{g/g}$ TOC, which approaches levels found at the Permian-Triassic boundary [11].

Chapter 4

Compound-specific isotope analysis (CSIA)

4.1 Results of CSIA analyses

Compound-specific isotope analysis was undertaken in order to obtain more information about relationships between compounds and about sources of specific compounds. Attention was focused on the primary production biomarkers pristane and phytane and the *n*-alkanes. Data are presented at the bottom of Table C.2 and plotted in Figure D-11, with δ_{toc} as a reference.

Several immediate inferences about the source of these compounds can be drawn from this isotopic information. Once again, the sample at -4.0 m exhibits anomalous characteristics compared to the rest of the section. Isotope ratios of its *n*-alkanes, pristane and phytane are all 2 to 3‰ more enriched than in its nearest neighbor. In the early Jurassic, average marine organic carbon was significantly depleted in ^{13}C relative to terrigenous organic matter[15, 44]. The average δ value was -30‰, compared to -22‰ today. Thus, the relative isotopic enrichment of the sample at -4.0 m supports the conclusion that organic matter from this sample has a dominantly terrigenous source.

Above this sample, however, the isotopic compositions of *n*-C₁₇, *n*-C₁₈, pristane and phytane vary little through the middle of the section. Pristane and phytane vary

together with a constant offset, and can thus be attributed to a common source. This source is most likely photosynthetic producers, as these compounds are thought to be largely derived from the phytol side-chain of chlorophyll [13].

The striking characteristic of this section is that the isotopic composition of the biomarkers analyzed do not vary with the bulk δ_{toc} . δ_{toc} and δ values of specific compounds must therefore represent different sources, except in the sample at -4.0 m.

The upper part of the section displays a change in ‘isotopic ordering’. Until the upper *exaratum* subzone, pristane and phytane are consistently 1 to 2‰ heavier than $n\text{-C}_{17}$ and $n\text{-C}_{18}$, consistent with known biosynthetic offsets in algae and cyanobacteria [30]. In the two samples above height +6.0 m, however, while $n\text{-C}_{17}$ and $n\text{-C}_{18}$ remain relatively steady at 32 to 33‰, pristane and phytane become extremely depleted, at -36 and -35‰, respectively. In these samples, pristane and phytane become notably lighter than the n -alkanes, causing a change in ‘isotopic ordering’. No known biosynthetic pathway can produce such isotopic ordering, though this relationship has been found in Proterozoic sediments [26, 27], as well as around other OAE’s, including the Permian-Triassic boundary [11]. This switch has previously been attributed to extensive heterotrophy in the water column, resulting in isotopically enriched n -alkanes relative to pristane and phytane.

4.2 Chromatography of desulfurized samples

To insure that the pristane and phytane observed in the free fraction were in fact the dominant marine signal, we desulfurized four samples and analysed the resulting saturated hydrocarbons by GC-MS. The sample at +3.2 m, shown in Figure D-12, which is at the maximum of organic carbon abundance, shows low concentrations of short chain marine n -alkanes and isoprenoids relative to UCM and long chain alkanes and more complex compounds. Thus, we feel confident that the isotopic signal from pristane and phytane in the extractable fraction is representative of a marine source.

4.3 The isotopic composition of terrestrial organic matter

Figure D-13 shows the isotopic compositions of all the n -alkanes of three representative samples. Short chain n -alkanes (n -C₁₇ to n -C₂₁) are probably most representative of algal inputs, whereas long chain n -alkanes (n -C₂₇ to n -C₃₁) contain input from higher plant waxes [34]. Results reveal distinctly different isotopic compositions for the short and long chain n -alkanes, indicating that algal inputs were depleted by 1 to 2 ‰ relative to plants.

Using n -C₂₇ to n -C₃₁, we can infer the change in isotopic composition of higher plants through this event. Figure D-14 shows their isotopic composition as a function of stratigraphic height. Like the short chain alkanes, n -C₂₇ to n -C₃₁ vary only slightly. In direct contrast, Hesselbo (2000) [16] reported a 6‰ change in the isotopic composition of fossil wood over the same stratigraphic range as this study. The former study contained no supporting evidence to assure that this change was not a result of any of the numerous parameters that can affect δ_t , such as plant type, plant part or temperature [31]. The isotopic composition of the lowest sample, however, is anomalously heavy compared to the rest of the section. Because this sample is different in biomarker ratios and bulk organic matter composition as well, we believe this change is due to a change in vegetation and not a secular change in the isotopic composition of the atmosphere.

Chapter 5

Discussion

5.1 Estimate of δ_m , the isotopic composition of marine organic carbon

As discussed in Section 2.1, samples in the upper *tenuicostatum* zone of the studied section contain significant inputs of terrestrial organic matter. Land-derived plant material, which contains different isotopic characteristics to marine material, may mask the true nature of the excursion in bulk δ_{toc} .

Using new data from this study, we can estimate the isotopic effect of the terrigenous input on the bulk δ_{toc} . Here, a simple model is presented, similar in approach to that of Jasper and Gagosian (1990) [17], where a mixed source of bulk organic matter is assumed, containing a weighted average of marine and terrigenous end members. The isotopic composition of bulk organic carbon, δ_{toc} , is given by

$$\delta_{\text{toc}} = f_t \delta_t + (1 - f_t) \delta_m, \quad (5.1)$$

where δ_{toc} is the isotopic composition of bulk organic matter, f_t is the fraction of organic matter that is terrigenous, δ_t is the isotopic composition of terrestrial organic matter, and δ_m is the isotopic composition of marine organic matter. Solving for δ_m yields

$$\delta_m = \frac{\delta_{\text{toc}} - f_t \delta_t}{1 - f_t}. \quad (5.2)$$

Thus, to assess the effect of the terrigenous matter on bulk δ_{toc} , we require knowledge of δ_{toc} , δ_t and f_t . δ_{toc} was measured directly in this study, but the other two require some further calculations.

As discussed above, isotopic compositions of $n\text{-C}_{27}$ to $n\text{-C}_{31}$ may be used as a proxy for δ_t . These long chain alkanes, however, are remnants of plant waxes, whose isotopic composition varies from bulk terrestrial organic carbon due to further fractionation in their production. A constant offset between waxes and bulk plant matter has been found to be between 5 and 6‰ [33]. Thus we add a constant 5.5‰ to the average of $\delta_{n\text{C}-27}$ to $\delta_{n\text{C}-31}$ to estimate δ_t across the section.

Regression analysis of HI on f_t was used to determine f_t for all samples across the section. The four samples analyzed by organic petrology were the basis of the regression line. Then, values of HI were placed on that line to calculate the equivalent f_t . Results of these calculations are shown in Table C.1.

Using these estimates of δ_t and f_t for all samples in the section, the isotopic composition of marine organic carbon, δ_m , could then be estimated. Values for f_t , δ_t and δ_{toc} were inserted into Equation (5.2) to yield a value for δ_m . The uncertainty in the regression line was used to calculate uncertainties in the values of f_t estimated from measurements of HI. In turn, the uncertainties in δ_t and f_t were combined in a conventional error-propagation treatment to determine the uncertainties in computed values of δ_m .

In addition, ϵ , the fractionation between marine inorganic and organic carbon, defined as

$$\epsilon = \delta_{\text{carb}} - \delta_m, \quad (5.3)$$

was calculated for the whole section. For δ_{carb} , we chose to use $\delta_{\text{belemnites}}$ from McArthur (2000) [28], for reasons discussed in Section 2.2.

Figure D-15 shows a summary of our best estimates of δ_m , δ_t , δ_{carb} and ϵ through

the Hawsker Bottoms section, as well the error ascribed to our calculation of δ_m and ϵ . These plots show a rough parallel between the δ_m and the δ_{carb} curves from 0 to +6 m, reflected in an ϵ value of about -34‰ through this interval. Below 0 m, however, a trend in δ_m is difficult to resolve due to the uncertainty in these measurements. The large error in the sample at -4.0 m is due to the strongly dominant component of terrestrial organic matter in that sample. Because there is little variation in δ_{carb} , δ_t or the isotopic compositions of the primary production biomarkers below 0 m, we believe that with the exception of the sample of -2 m, the isotopic composition of total marine organic carbon hovers between -31 and -33 ‰.

In summary, we conclude that the authentic isotopic signals - ϵ , δ of pristane, phytane and marine *n*-alkanes, and δ_t - remain flat through this OAE where the bulk organic signal undergoes a large change.

5.2 Periodic euxinia

Because we have found no evidence for significant isotopic variation on land or in the ocean, we must infer that there were no major redistributions of carbon in the ocean-atmosphere system during the Toarcian OAE. Therefore, oceanic overturn or large input of methane are not plausible explanations for this event. This deposition of black shales was a result of periodic episodic euxinia, which resulted in the increased preservation of organic matter. We believe that this event was not a large, one-time occurrence, but a characteristic response to paleogeography and oceanic circulation patterns of the Mesozoic.

The presence and widespread distribution of aryl isoprenoids, which require euxinia for their production, indicate that a sulfidic photic zone was a common occurrence, before, during and after the OAE at Hawsker Bottoms and in other sections [43]. Isorenieratane maximum abundance is near the maximum in TOC, implying that strengthening euxinia was responsible for increase in organic carbon burial. The presence of benthic fauna, and low TOC abundance before the event, however, leads us to a conclusion reached in Schouten et. al. (2000) [43], that this euxinia was

periodic prior to the main deposition of black shales. Even during the most intense deposition, both benthic fauna and short periods without lamination are present, suggesting that there were brief oxic events interrupting the OAE.

The occurrence of such frequent shifts into and out of anoxia, as well as several oceanic anoxic events in the Mesozoic, infers that the paleogeography of the time may have caused the oceans to be prone to anoxia. Quantitative models have predicted that paleogeography which included large spans of epicontinental seas could result in a change in oceanic circulation such that oceanic deep waters are formed in tropical areas [6, 49]. In such a scenario, periods of large evaporation due to global warming would cause oceanic deep water to be warm and saline rather than cold and oxygenated, as they are today. Sarmiento et. al. (1988) [41] determined that oxygen concentrations in the waters which feed the deep ocean exert the major control on ocean anoxia. Thus, an earth with the paleogeography similar to that of the Toarcian, with low-latitude shallow seas, would be particularly susceptible to short periods of ocean anoxia. Bailey et. al.(2003) [1] and McElwain et. al. (2005) [29] identified a global warming and significant CO₂ increase in the Toarcian, which possibly jump-started this shift into anoxia.

Our findings do not support a major event of oceanic overturn, as supported in former studies [24, 43]. These former models were based on apparent negative excursions in the isotopic composition of bulk organic carbon, bulk carbonate carbon and several specific organic compounds. Our results differ starkly. Isotopic composition of surface-water biomarkers show no negative change. Authentic carbonate and organic carbon bulk signals were altered by diagenesis and terrigenous input, respectively, and reveal no negative excursion. The isotopic composition of plant wax biomarkers, which should roughly vary with the isotopic composition of the atmosphere, showed little variation through the section. Evidence for major oceanic overturn across the Toarcian OAE is absent.

5.3 Implications for the methane hypotheses

Hesselbo et. al. (2000) [16] postulated that coincident negative excursions in bulk organic carbon and fossil wood isotopes signified a common, major perturbation to the oceanic and atmospheric carbon reservoirs in the form of a release of 1500 to 2700 Gt of methane hydrates. Beerling et. al. (2002) [2] increased this estimate to a release of 5000 Gt of methane based on modeling results. Most recently, however, McElwain, Wade-Murphy and Hesselbo (2005) [29] found that the catastrophic release of methane hydrates is not supported by their results. As an alternative, however, they offer that the release of thermogenic methane due to magmatic intrusion into Gondwanan coals as a more plausible hypothesis.

Biomarker, CSIA and bulk carbon isotopic results from our investigation, however, do not support the presence of large amounts of methane in the water column. Predominantly, the abundance of the 3β -methylhopane biomarker, an indicator of methanotrophs, in relation to both C_{30} hopane or 2α -methylhopane, does not change significantly through the section. Methanotrophic bacteria or archaea would be expected in the event of high concentrations of methane in the water column. There is no hint of extreme depletion or a significant change in the isotopic composition in the short or long chain n -alkanes, or pristane and phytane, as one might expect from an ocean and atmosphere strongly effected by methane and its anaerobic oxidation. The total marine organic carbon record does not demonstrate a large and rapid negative excursion, and carbonate records from belemnite rostra across the Toarcian OAE show no negative excursion in δ_{carb} .

The most well-documented release of methane hydrates in earth history, the Late Paleocene Thermal Maximum (LPTM), is recorded by a negative excursion in *both* δ_{carb} and δ_{toc} (e.g. [9]). Hesselbo et. al. postulated that high CO_2 production from methane oxidation would cause increased acidity in the water column and thus increased carbonate dissolution. Though this explanation is a plausible one, it is not clear why the apparent negative excursion in carbonate at the LPTM is so strong, and why such a change would not be recorded across the Toarcian.

Chapter 6

Conclusion

Bulk carbon, biomarker and compound-specific isotopic analyses, have shown that none of the authentic marine signals undergo significant variation across the Toarcian OAE. The isotopic compositions of surface ocean biomarkers and higher plant biomarkers, as well as the fractionation between inorganic and organic carbon remain relatively steady, indicating that there were no major redistributions of carbon in the ocean-atmosphere system. Our results differ significantly from other studies. We strongly believe that apparent negative isotopic excursions in organic and carbonate carbon were the result of compositional changes of organic matter and diagenesis, respectively. This investigation highlights the importance of using caution in the interpretation of bulk carbon isotopic signals to infer large changes in the carbon cycle.

Appendix A

Abbreviations

Table A.1: Abbreviation for compounds identified in Figures D-4 and D-5.

<i>Abbreviation</i>	<i>Compound</i>
Steranes	
C ₂₇ steranes	
C ₂₇ diast. β _α 20S/R	13β(H),17α(H)-diacholestane (20S/R)
αααS/R	5α(H),14α(H),17α(H)-cholestane (20S/R)
αββS/R	5α(H),14β(H),17β(H)-cholestane (20S/R)
C ₂₈ steranes	
C ₂₈ diast. β _α 20S/R	13β(H),17α(H)-24-methyldiacholestane (20S/R)
αααS/R	5α(H),14α(H),17α(H)-24-methylcholestane (20S/R)
αββS/R	5α(H),14β(H),17β(H)-24-methylcholestane (20S/R)
C ₂₉ steranes	
C ₂₉ diast. β _α 20S/R	13β(H),17α(H)-24-ethyldiacholestane (20S/R)
αααS/R	5α(H),14α(H),17α(H)-24-ethylcholestane (20S/R)
αββS/R	5α(H),14β(H),17β(H)-24-ethylcholestane (20S/R)
C ₃₀ steranes	
C ₃₀ diast. β _α 20S/R	13β(H),17α(H)-24-propyldiacholestane (20S/R)
αααS/R	5α(H),14α(H),17α(H)-24-propylcholestane (20S/R)
αββS/R	5α(H),14β(H),17β(H)-24-propylcholestane (20S/R)
Hopanes	
C ₂₇ hopanes	
Ts	18α(H)-22,29,30-trisnorneohopane
Tm	17α(H)-22,29,30-trisnorhopane
C ₂₈ hopanes	
29,30 BNH	17α(H),21β(H)-29,30-bisnorhopane
28,30 BNH	17α(H),18α(H),21β(H) and 17β(H),18α(H),21α(H)-28,30-bisnorhopane
C ₂₉ hopanes	
C ₂₉ diahopane	17α(H)-diahopane
C ₂₉ H	17α(H),21β(H)-30-norhopane
C ₂₉ Ts	18α(H),21β(H)-30-norneohopane
C ₂₉ H	17β(H),21α(H)-30-norhopane
C ₃₀ hopanes	
C ₃₀ diahopane	17α(H)-diahopane
C ₃₀ H	17α(H),21β(H)-hopane
C ₃₀ moretane	17β(H),21α(H)-hopane
C ₃₁ hopanes	
C ₃₁ diahopane	17α(H)-diahopanes
C ₃₁ αβ-22S/R	17α(H),21β(H)-homohopane (22S/R)
C ₃₂ hopanes	
C ₃₂ αβ-22S/R	17α(H),21β(H)-bishomohopane (22S/R)

Appendix B

Definitions of biomarker ratios

Table B.1: Calculation of biomarker ratios shown in Table C.2 and Figure D-8.

<i>Ratio name</i>	<i>Definition</i>	<i>GC-MS ion / reaction</i>
1 Ts/(Ts+Tm)		MRM 370→191
2 Hop maturity index	$C_{31}H \frac{22S}{22S+22R}$	MRM 426→191
3 Ster maturity index	$C_{29}St \frac{20S}{20S+20R}$	MRM 400→217
4 MPI (methylphenanthrene index) ¹	$\frac{1.89 \times (3MP+2MP)}{P+1.26 \times (9MP+1MP)}$	m/z 192 of aromatic full scan
5 prist / phyt	pristane / phytane	GC-MS full scan of MSNA fraction
6 sters / hops	$\frac{\Sigma C_{27}-C_{29}St}{C_{27}Tm+28.30BNH+C_{29}H+C_{30}H+C_{31}(S+R)H}$	MRM M ⁺ →191 and 217
7 %C27 St	$\frac{\Sigma C_{27}St}{\Sigma C_{27}-C_{29}St} \times 100$	MRM M ⁺ →217
8 %C29 St	$\frac{\Sigma C_{29}St}{\Sigma C_{27}-C_{29}St} \times 100$	MRM M ⁺ →217
8 homohopane index	$\frac{C_{35}(S+R)}{\Sigma C_{31}-C_{35}H} \times 100$	MRM M ⁺ →191
10 2αMeH index	$\frac{2\alpha C_{31}MeH}{2\alpha C_{31}MeH+C_{30}H} \times 100$	MRM 426→205
11 3βMeH index	$\frac{3\beta C_{31}MeH}{3\beta C_{31}MeH+C_{30}H} \times 100$	MRM 426→205
12 gammacerane index	$\frac{\text{gammacerane}}{C_{30}H} \times 100$	MRM 412→191
13 4-Methylsterane index	$\frac{4Me-C_{30}St(R)}{C_{29}St(R)} \times 100$	MRM 412→231

Appendix C

Tables

Table C.1: Bulk geochemical data for the sample suite.

height ¹ (m)	sample name	TOC %	HI mg HC/g TOC	T _{max} °C	PI ²	δ _{toc} ‰	f _{terrestrial} measured, %	f _{terrestrial} calculated ³ , %
+6.9	ENR005	5.2	343	432	0.17	-27.4		40
+6.1	ENR015	4.0	395	433	0.18	-27.5		24
+5.9	ENR004	4.9	330	434	0.18	-26.9	40	45
+5.1	ENR003	4.7	331	436	0.17	-28.5		44
+4.4	ENR002	4.7	403	435	0.15	-28.8		22
+3.2	ENR001	10.7	431	437	0.14	-31.0	25	13
+2.0	ENR006	8.5	435	436	0.12	-32.2		12
+1.2	ENR007	6.6	417	434	0.12	-31.0		18
+0.4	ENR008	6.8	324	429	0.16	-30.8		46
+0.3	ENR013	5.7	366	437	0.11	-31.0	25	33
-0.6	ENR012	5.3	341	436	0.12	-30.3		41
-1.0	ENR011	3.4	259	433	0.18	-27.3		67
-2.0	ENR010	4.4	305	440	0.14	-26.8		52
-2.7	ENR017	2.2	444	437	0.15	-26.6		9
-3.4	ENR016	2.0	220	438	0.13	-25.9	80	79
-4.0	ENR009	1.7	240	440	0.12	-25.9		72
-4.5	ENR018	1.9	182	438	0.12	-25.8		91
-5.3	ENR019	1.7	192	439	0.11	-26.0		87

¹Based on stratigraphy from Ref. [28] and subsequently Ref. [21].

²The production index (PI) is a measure of thermal maturity and is calculated as $PI = S_1/(S_1+S_2)$, where S_1 and S_2 are peak heights from Rock-Eval pyrolysis.

³f_{terrestrial} was calculated for all the samples using regression analysis as described in Section 5.1.

Table C.2: Biomarker ratios and compound-specific isotope data for sample suite (shown in stratigraphic order from lowest to highest. For parameter definitions and ratio calculations, see Appendix B).

sample no. height (m) ^a	ENR009	ENR010	ENR011	ENR013	ENR008	ENR007	ENR006	ENR001	ENR002	ENR003	ENR004	ENR005
	-4.0	-2.0	-1.0	0.3	0.4	1.2	2.0	3.2	4.4	5.1	5.9	6.9
maturity parameters												
1	Ts/(Ts+Tm)	0.46	0.57	0.60	0.56	0.57	0.56	0.55	0.56	0.55	0.59	0.56
2	Hop maturity index	0.60	0.60	0.60	0.59	0.59	0.60	0.59	0.60	0.60	0.60	0.60
3	Ster maturity index	0.53	0.51	0.52	0.51	0.51	0.52	0.51	0.51	0.52	0.52	0.51
4	MPI	0.49	0.53	0.55	0.53	0.49	0.50	0.52	0.49	0.54	0.53	0.53
source indicators												
5	prist / phyt	2.1	0.8	1.1	0.8	1.0	1.1	0.9	1.1	1.0	1.0	0.9
6	ster / hop	0.54	1.71	1.94	1.84	1.84	2.05	1.72	1.77	1.94	1.93	2.18
7	%C27 St	26.5	33.0	32.9	33.2	33.2	35.6	32.7	32.7	32.1	32.1	32.3
8	%C29 St	52.2	43.9	43.9	44.2	43.1	41.4	43.4	44.4	44.1	45.1	43.8
9	homohopane index (%)	3.6	7.1	7.0	6.8	7.3	6.9	7.6	6.9	8.1	7.4	6.7
10	2 α MeH index	2.4	2.1	2.1	1.8	2.0	1.6	2.1	1.8	1.9	1.8	1.2
11	3 β MeH index	2.2	1.8	1.5	1.4	1.8	1.5	1.8	1.7	1.8	1.7	1.7
12	gammacerane index	0.85	2.47	2.48	2.55	3.13	2.85	3.09	2.66	2.79	2.84	3.00
13	4-Methylsterane index	0.25	0.58	0.58	0.63	0.54	0.61	0.64	0.57	0.63	0.55	0.62
14	isorenieratane (ng/g TOC)	26.8	287.6	170.0	150.8	239.3	140.7	139.8	184.0	108.3	985.8	270.0
Stable carbon isotopic compositions of different biomarkers, in units of ‰, with a pooled standard deviation of 0.3‰												
15	δ_{pristane}	-30.3	-32.4	-32.3	-31.1	-32.6	-32.7	-32.0	-32.1	-33.0	-33.2	-35.0
16	δ_{phytane}	-29.0	-32.2	-31.9	-31.9	-32.0	-32.1	-31.8	-31.6	-32.3	-32.2	-35.0
17	$\delta_n\text{-C17}$	-31.3	-33.0	-33.0	-32.6	-33.3	-33.0	-33.3	-34.1	-33.3	-33.9	-32.7
18	$\delta_n\text{-C18}$	-30.4	-32.9	-32.9	-32.8	-33.2	-32.9	-33.1	-33.9	-33.1	-33.6	-32.5
19	$\delta_n\text{-C19}$	-30.5	-32.9	-32.4	-32.8	-33.1	-32.8	-33.1	-33.8	-33.2	-33.6	-32.5
20	$\delta_n\text{-C20}$	-30.3	-33.0	-32.9	-32.9	-33.2	-32.8	-33.0	-33.6	-33.1	-33.5	-32.6
21	$\delta_n\text{-C21}$	-29.8	-32.6	-32.7	-32.8	-32.9	-32.8	-32.9	-33.3	-33.0	-33.3	-32.5
22	$\delta_n\text{-C22}$	-29.6	-32.4	-32.9	-32.7	-33.1	-32.8	-33.0	-33.3	-33.1	-33.3	-32.6
23	$\delta_n\text{-C23}$	-29.1	-32.1	-32.6	-32.5	-32.9	-32.7	-32.8	-33.0	-32.9	-33.0	-32.5
24	$\delta_n\text{-C24}$	-28.9	-31.9	-32.7	-32.4	-33.1	-32.9	-32.9	-33.1	-32.9	-33.1	-32.8
25	$\delta_n\text{-C25}$	-28.8	-31.7	-32.4	-32.6	-32.7	-32.5	-33.1	-32.5	-32.8	-32.8	-31.8
26	$\delta_n\text{-C26}$	-28.5	-31.4	-32.2	-32.1	-32.5	-32.5	-32.5	-32.4	-32.5	-32.5	-32.3
27	$\delta_n\text{-C27}$	-28.6	-31.2	-31.9	-31.8	-32.1	-32.2	-32.1	-31.8	-32.2	-32.0	-31.9
28	$\delta_n\text{-C28}$	-28.7	-30.9	-31.6	-31.6	-32.2	-32.1	-31.8	-31.6	-32.1	-31.7	-31.7
29	$\delta_n\text{-C29}$	-28.7	-31.0	-31.7	-31.5	-32.1	-31.9	-31.2	-31.4	-31.9	-31.7	-31.7
30	$\delta_n\text{-C30}$	-29.9	-31.0	-31.8	-31.5	-32.0	-32.1	-31.0	-31.4	-32.1	-31.7	-31.9
31	$\delta_n\text{-C31}$	-29.7	-31.2	-31.7	-31.8	-31.8	-32.0	-30.8	-31.3	-32.0	-31.6	-31.6
32	$\delta_n\text{-C32}$	-30.6	-31.2	-31.4	-31.9	-31.7	-32.0	-30.5	-31.2	-32.0	-31.6	-31.9
33	$\delta_n\text{-C33}$	-30.0	-31.1	-31.5	-31.7	-31.9	-31.7	-30.1	-31.1	-31.8	-31.5	-32.0
34	average of $\delta_n\text{-C17-19}$	-30.7	-32.9	-32.8	-32.7	-33.2	-32.9	-33.2	-33.9	-33.2	-33.7	-32.5
35	average of $\delta_n\text{-C27-31}$	-29.1	-31.1	-31.7	-31.6	-32.0	-32.1	-31.4	-31.5	-32.0	-31.8	-31.1

^aStratigraphy from Refs. [28] and [21].

Appendix D

Figures

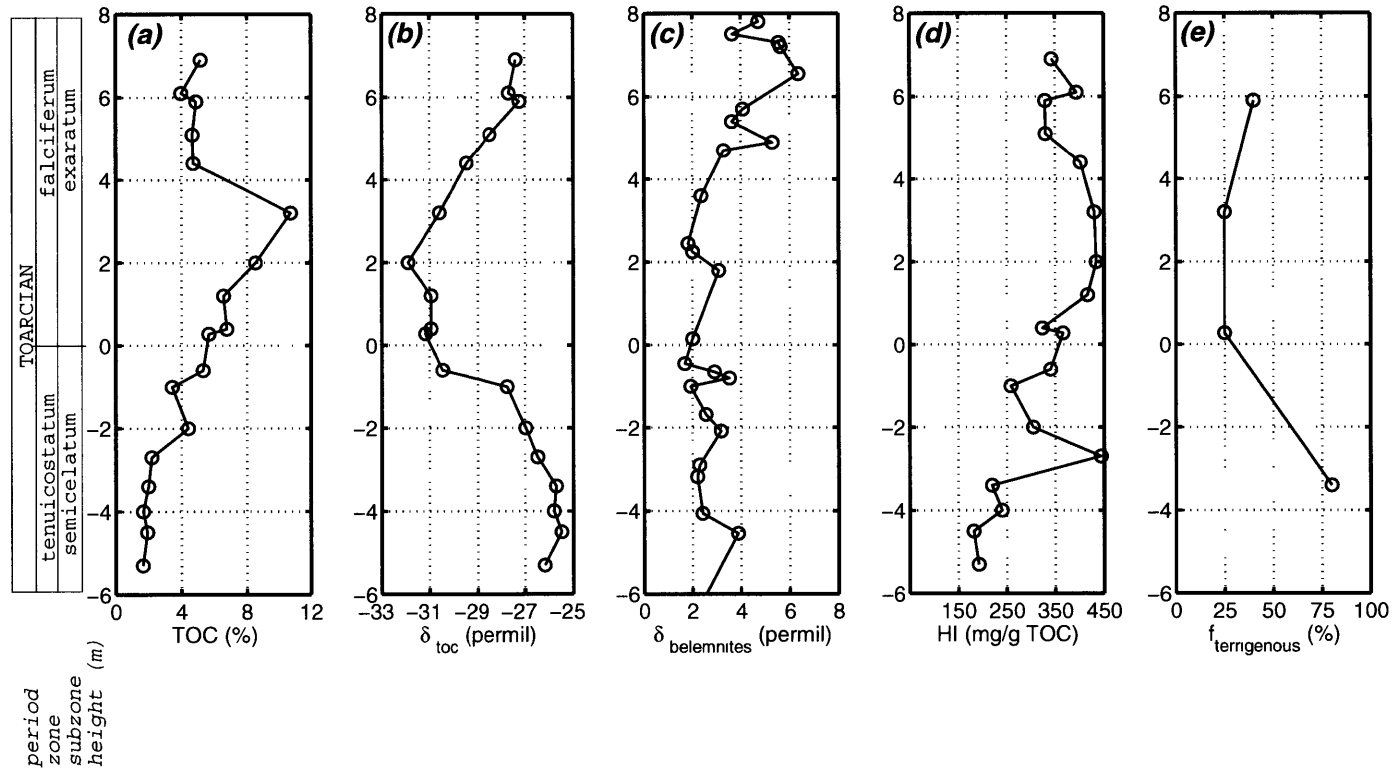
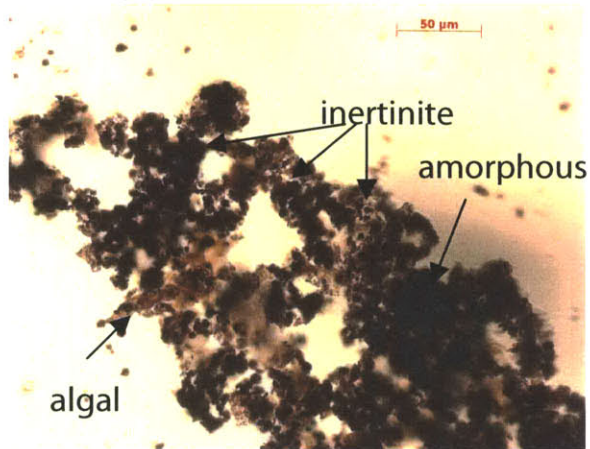


Figure D-1: Bulk data from the Hawsker Bottoms section of the Toarcian black shale deposition. Section is thought to last 500-700 k.y. [18, 1]. (a) Percent total organic carbon, (b) isotopic composition of total organic carbon, δ_{TOC} , (c) $\delta_{\text{belemnites}}$, isotopic composition of belemnite fossils, (d) hydrogen index (HI), and (e) percent of bulk composition that is terrigenous matter as determined through organic petrology. Chemostratigraphy as shown in Refs. [28] and [21]. $\delta_{\text{belemnites}}$ data from Ref. [28].

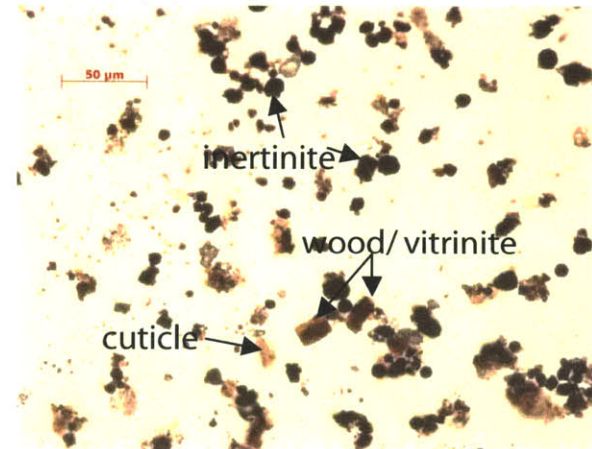
Marine

(a) +0.3 m, transmitted



Terrigenous

(b) -3.4 m, transmitted



(c) +3.2 m, blue light



(d) -3.4 m, blue light

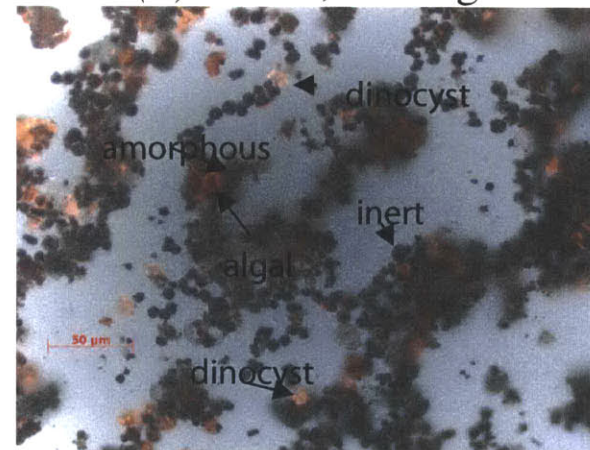


Figure D-2: Marine and terrigenous microfossils from the Jet Rock, Hawsker Bottoms, Yorkshire, England from kerogen isolates. Scale bars are 50 μm. (a) and (b) Comparison of marine (25% terrigenous) and woody (80% terrigenous) end members under transmitted light; and (c) and (d) in fluorescing light.

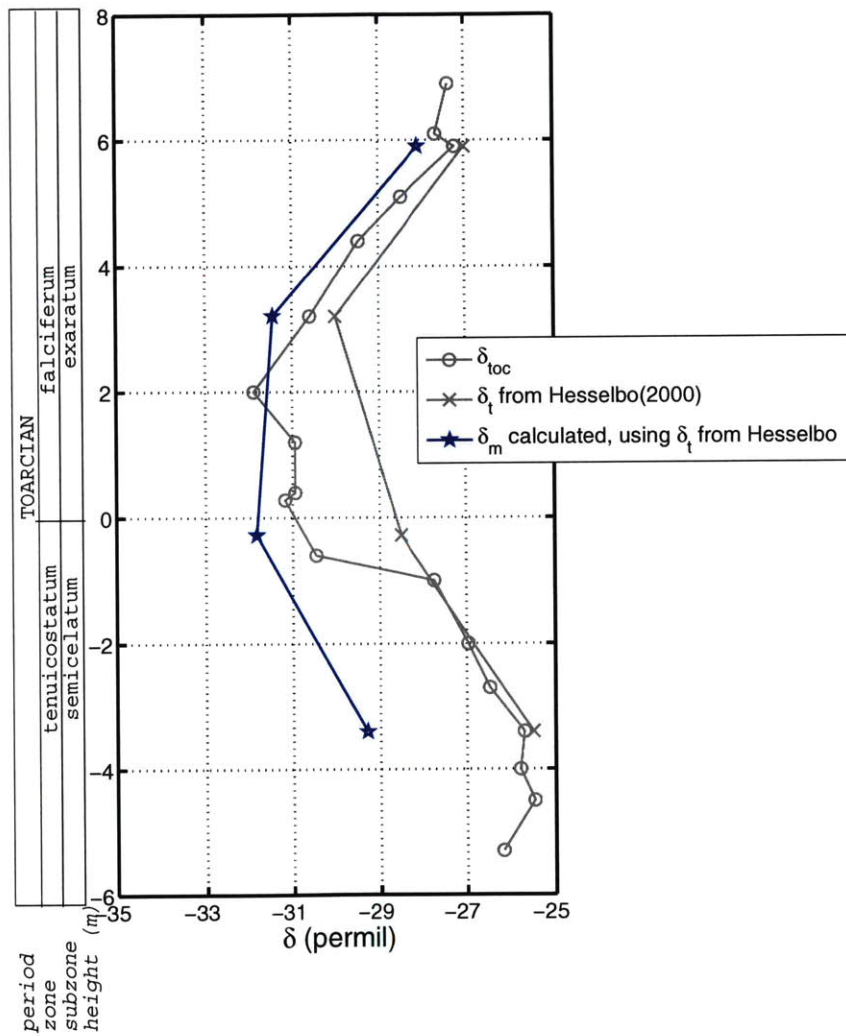


Figure D-3: Estimate of δ_m , the isotopic composition of marine organic carbon, using Equation (5.2) and different assumptions for the isotopic composition of terrestrial material, δ_t . Light grey lines are δ_{toc} and δ_t . δ_t data is from Hesselbo (2000) [16].

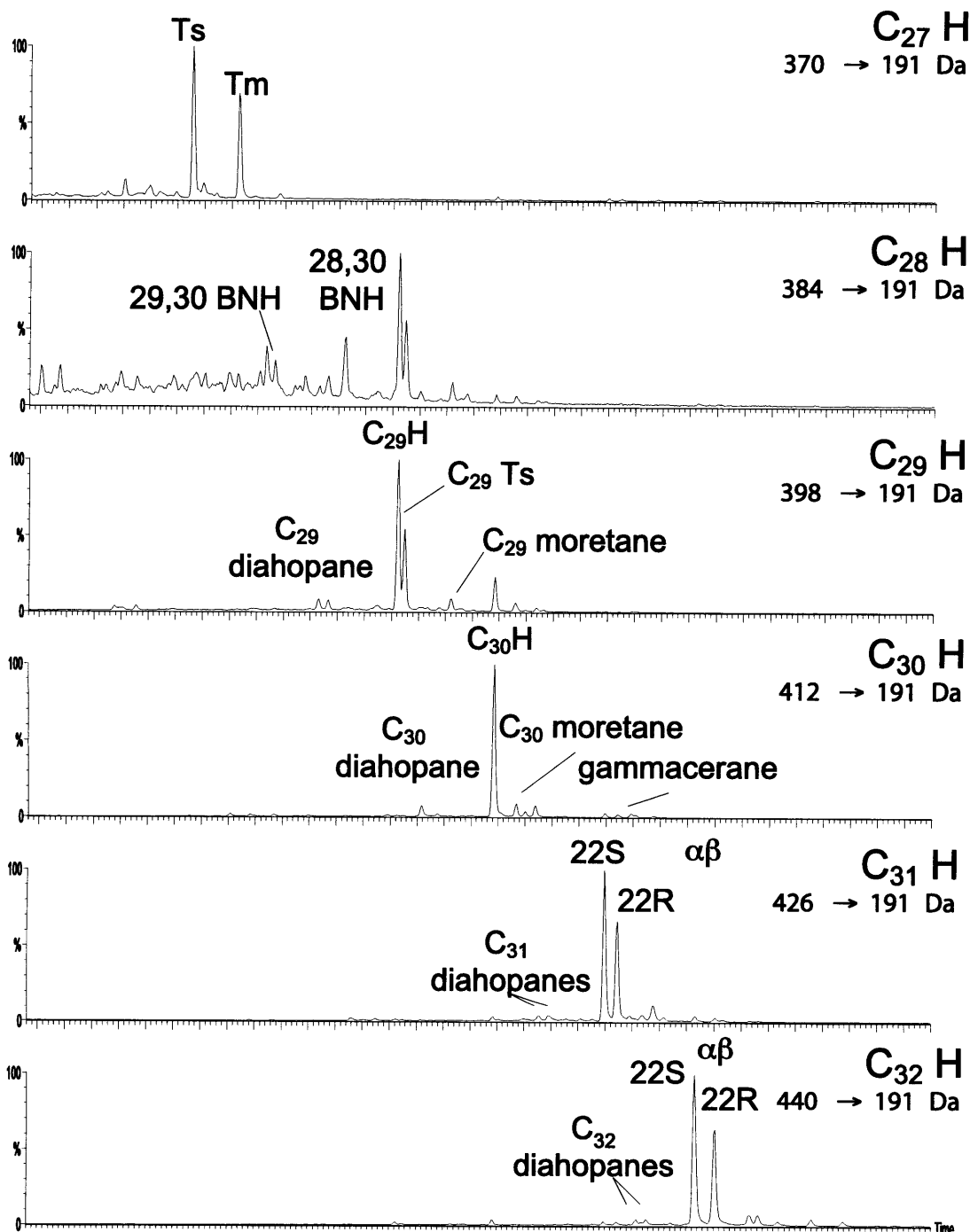


Figure D-4: Distribution of hopanes and other pentacyclic triterpanes in the saturated fraction of sample ENR004, at height +5.9 m. Data was obtained by GC-MS MRM transitions $M^+ \rightarrow 191$. Compounds are identified by carbon number and relative elution times. For abbreviation definitions, see Appendix A.

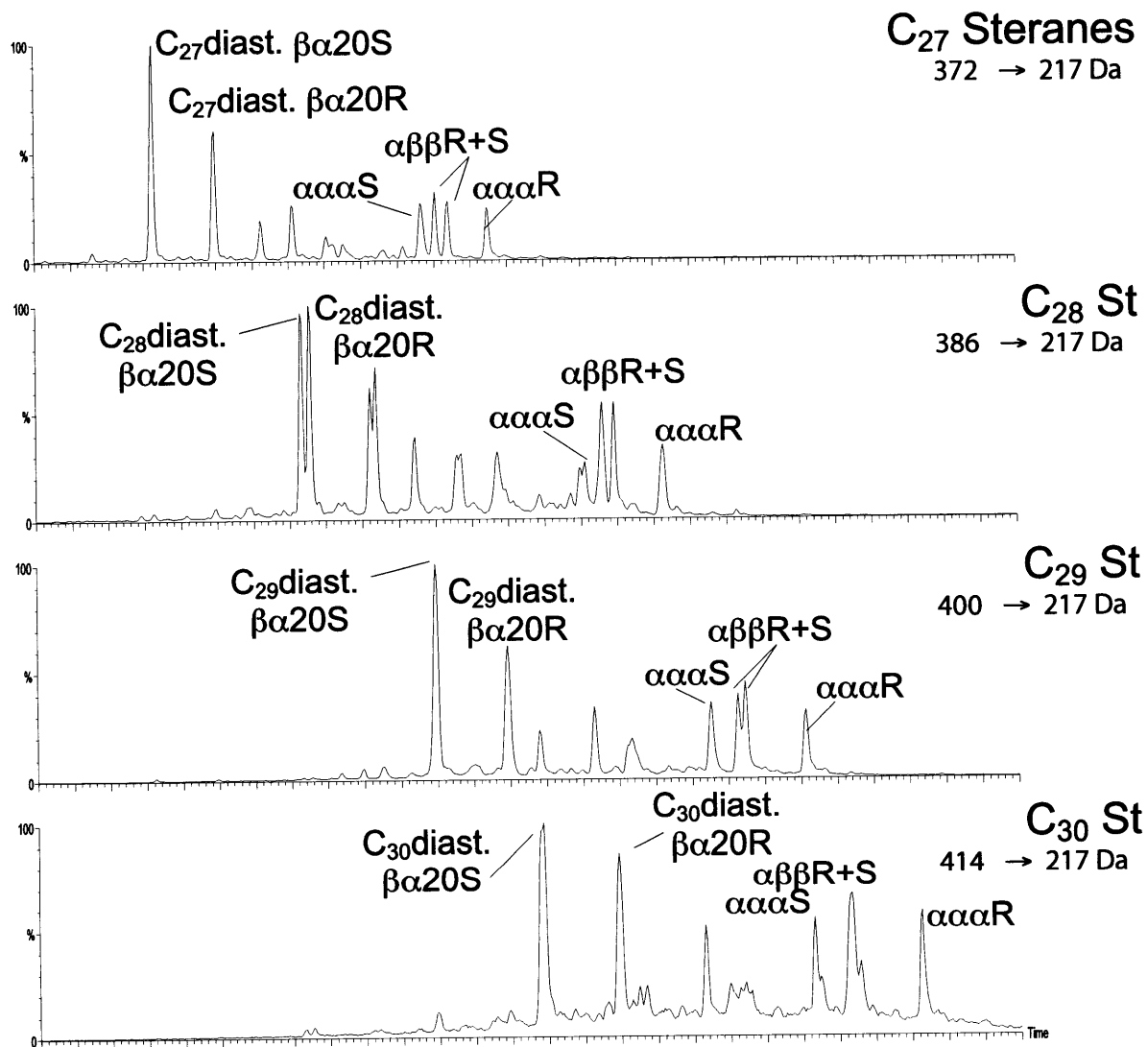


Figure D-5: Distribution of steranes in the saturated fraction of sample ENR004, at height +5.9 m. Data was obtained by GC-MS MRM transitions $M^+ \rightarrow 217$. Compounds are identified by carbon number and relative elution times. For abbreviation definitions, see Appendix A.

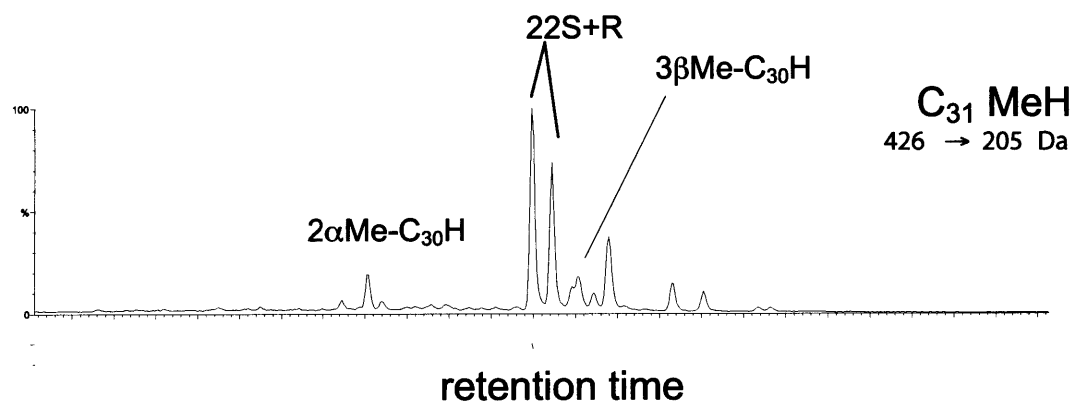


Figure D-6: Distribution of methylhopanes in the saturated fraction of sample ENR004, at height +5.9 m. Data was obtained by GC-MS MRM transitions 426→205. Compounds are identified by carbon number and relative elution times. For abbreviation definitions, see Appendix A.

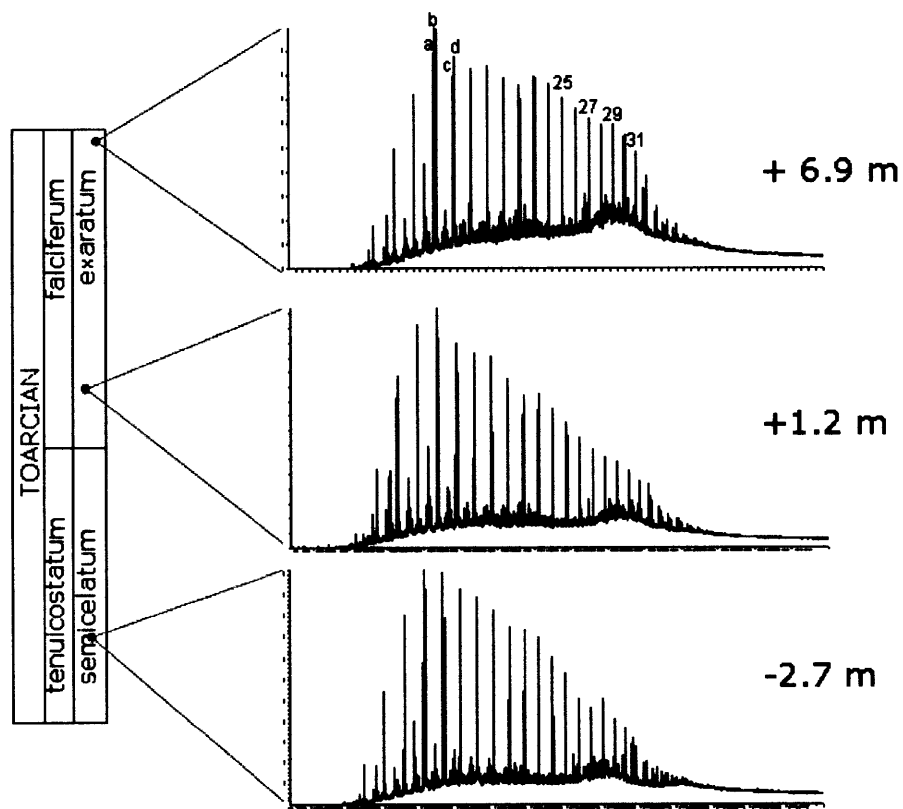


Figure D-7: Selected saturate fraction distributions through the section. Labeled peaks are (a) n -C₁₇ (b) pristane (c) n -C₁₈ and (d) phytane, along with n -C₂₅ through n -C₃₁.

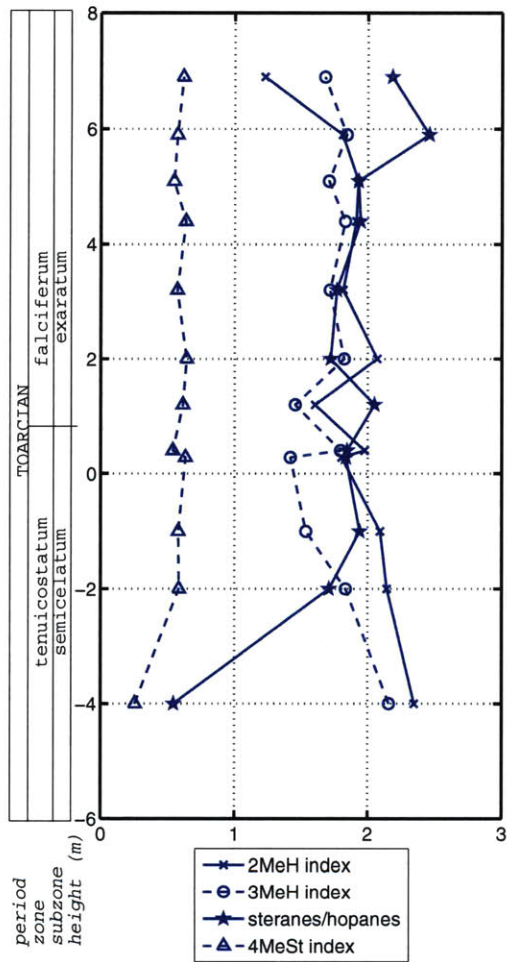


Figure D-8: Ratios of selected source biomarkers across the section. Calculations of biomarker parameters are found in Appendix B.

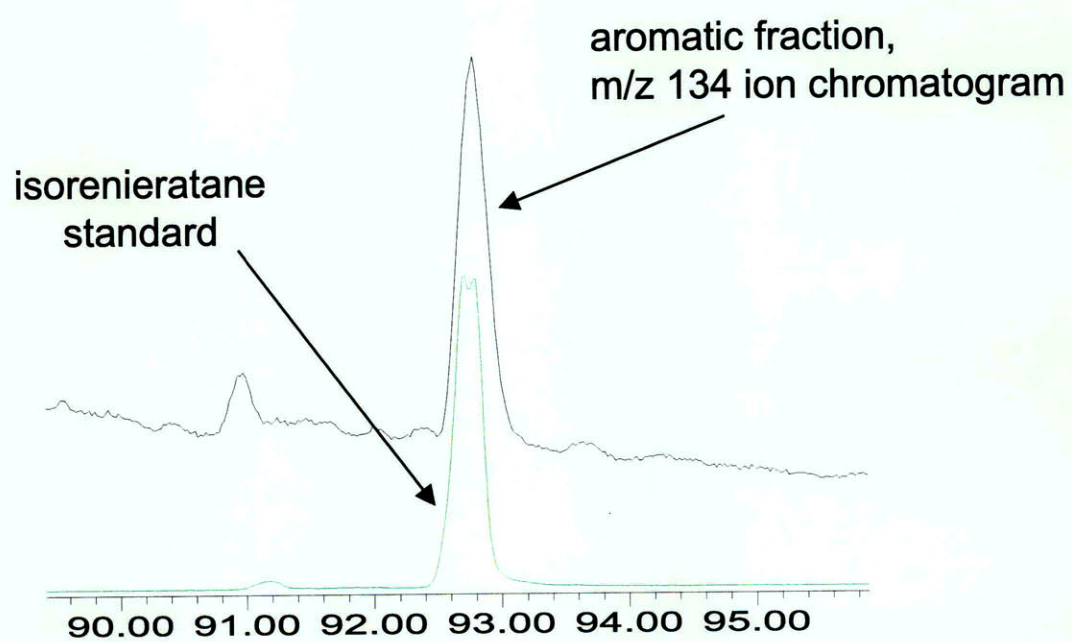


Figure D-9: Identification of isorenieratane, a biomarker for green sulphur bacteria, in sample ENR005, at height +6.9 m.

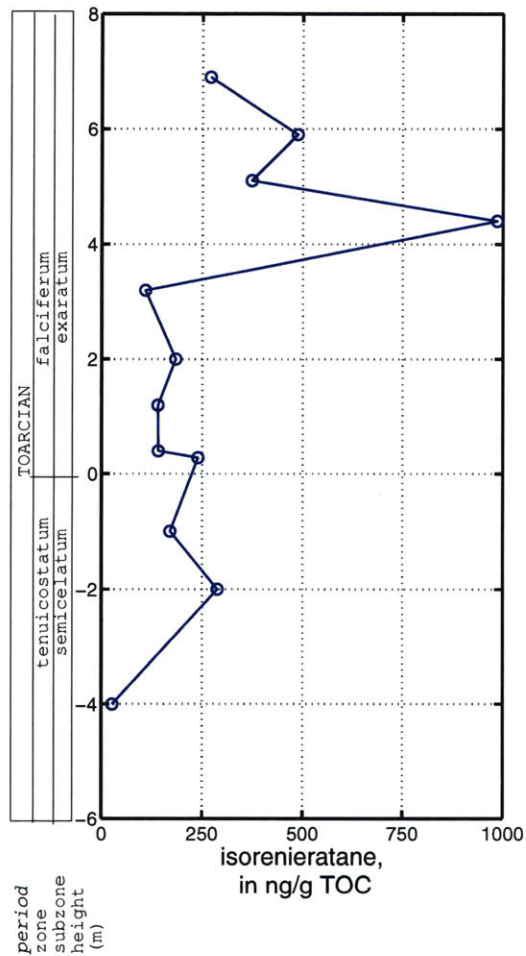


Figure D-10: Isorenieratane concentration normalized to total organic carbon abundance.

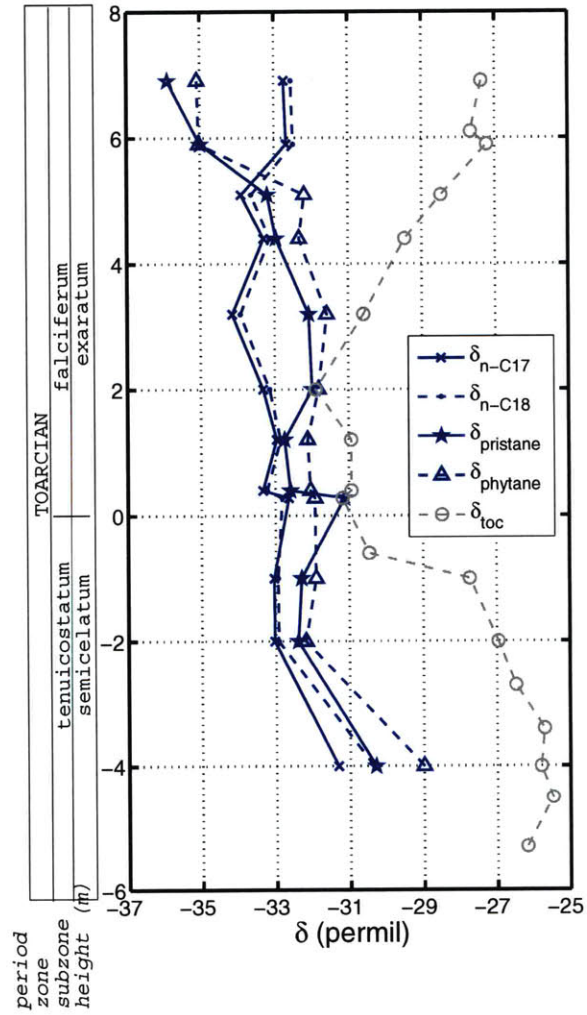


Figure D-11: $\delta^{13}\text{C}$ of $n\text{-C}_{17}$, $n\text{-C}_{18}$, pristane and phytane across the section.

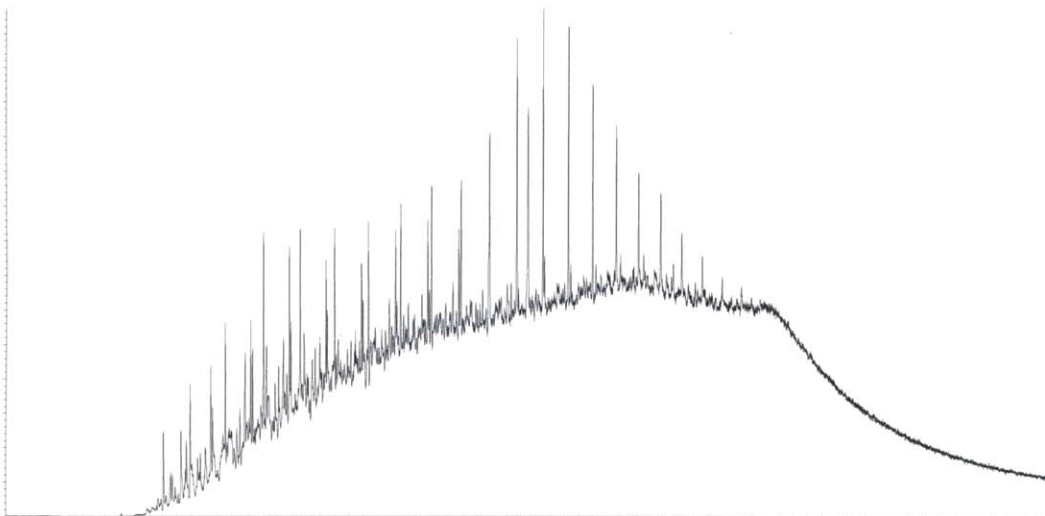


Figure D-12: Saturated fraction of desulfurized hydrocarbons, from sample ENR001 at +3.2 m.

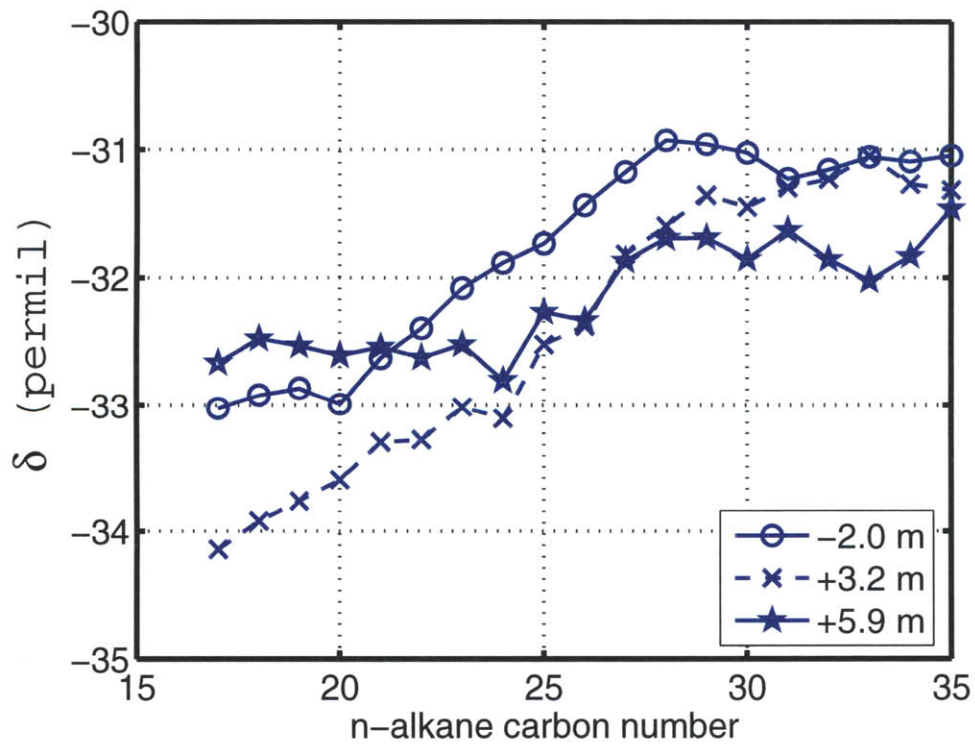


Figure D-13: $\delta^{13}\text{C}$ of all the n -alkanes of selected samples.

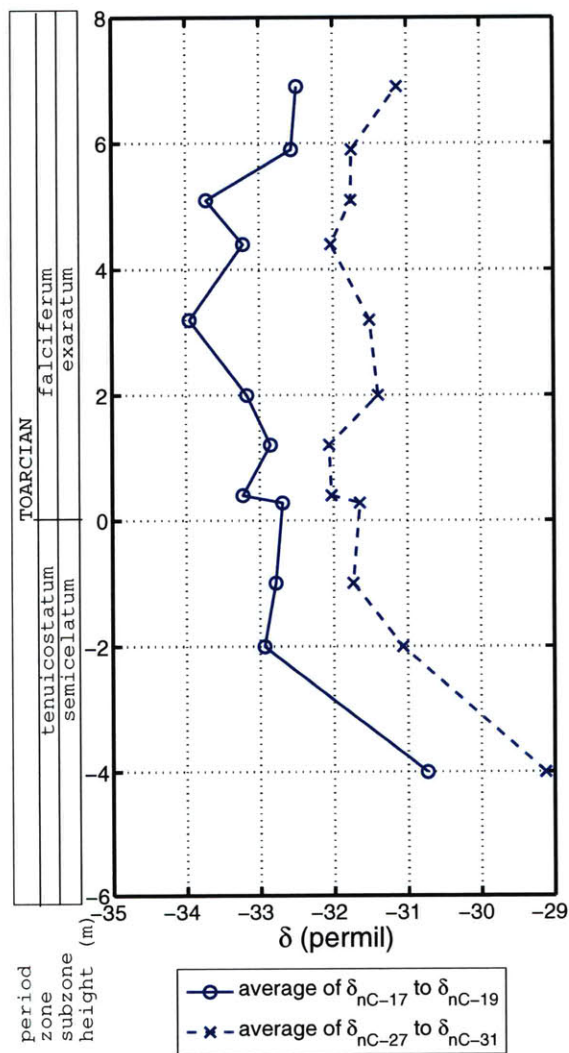


Figure D-14: Variation of the isotopic composition of short chain ($n-C_{17}$ to $n-C_{19}$) and long chain ($n-C_{27}$ to $n-C_{31}$) through the oceanic anoxic event.

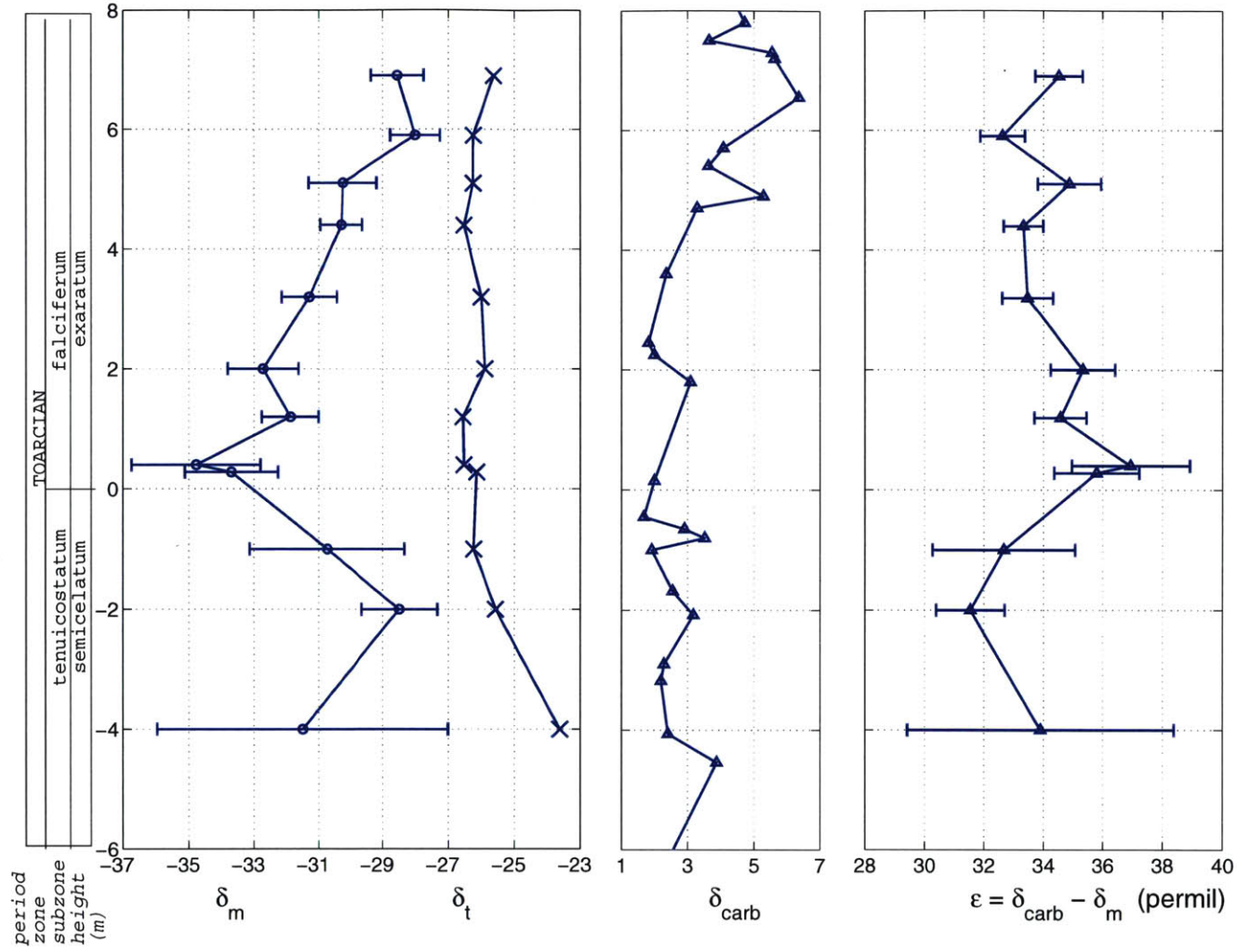


Figure D-15: Best estimates of δ_m , total marine organic carbon and the error ascribed to it, δ_t bulk terrestrial organic carbon, δ_{carb} marine carbonate and ϵ through the Hawsker Bottoms section. Calculations and assumptions are described in Section 5.1. δ_{carb} from McArthur (2000) [28].

Bibliography

- [1] T. R. Bailey, Y. Rosenthal, J. M. McArthur, B. van de Schootbrugge, and M. F. Thirlwall. Paleooceanographic changes of the late Pliensbachian - early Toarcian interval: a possible link to the genesis of an oceanic anoxic event. *Earth and Planetary Science Letters*, 212:307–320, 2003.

- [2] D. J. Beerling, M. R. Lomas, and D. R. Gröcke. On the nature of methane gas-hydrate dissociation during the Toarcian and Aptian oceanic anoxic events. *American Journal of Science*, 302:28–49, 2002.

- [3] C. L. Bjerrum, F. Surlyk, J. H. Callomon, and R. L. Slingerland. Numerical paleoceanographic study of the early Jurassic transcontinental Laurasian seaway. *Paleoceanography*, 16:390–404, 2001.

- [4] C. J. Boreham, I. H. Crick, and T. G. Powell. Alternative calibration of the Methylphenanthrene Index against vitrinite reflectance: Application to maturity measurements in oil and sediments. *Organic Geochemistry*, 12:289–294, 1988.

- [5] S. A. Bowden. *The molecular characterisation of sedimentary organic matter and petroleum by catalytic hydropyrolysis*. PhD thesis, University of Newcastle upon Tyne, 2003.

- [6] G. W. Brass, J. R. Southam, and W. H. Peterson. Warm saline bottom water in the ancient ocean. *Nature*, 296:620–623, 1982.

- [7] J. J. Brocks and R. E. Summons. Sedimentary hydrocarbons, biomarkers for early life. In H. D. Holland and K. Turekian, editors, *Treatise on Geochemistry*, pages 63–115. Elsevier, 2003.
- [8] W. E. Dean, M. A. Arthur, and G. E. Claypool. Depletion of ^{13}C in Cretaceous marine organic matter: Source, diagenetic or environmental signal. *Marine Geology*, 70:119–157, 1986.
- [9] G. R. Dickens, M. M. Castillo, and J. C. G. Walker. A blast of gas in the latest Paleocene: Simulating first-order effects of massive dissociation of oceanic methane hydrate. *Geology*, 25:259–262, 1997.
- [10] P. Farrimond, D. C. Stoddart, and H. C. Jenkyns. An organic geochemical profile of the Toarcian anoxic event in northern Italy. *Chemical Geology*, 111:17–33, 1994.
- [11] K. Grice, C. Cao, G. D. Love, M. E. Böttcher, R. J. Twitchett, E. Grosjean, R. E. Summons, S. C. Turgeon, W. Dunning, and Y. Jin. Photic zone euxinia during the Permian-Triassic superanoxic event. *Science*, 307:706–709, 2005.
- [12] A. Hallam. Estimates of the amount and rate of sea-level change across the Rhaetian-Hettangian and Pleinsbachian-Toarcian boundaries (latest Triassic to early Jurassic). *Journal of the Geological Society, London*, 154:773–779, 1997.
- [13] J. M. Hayes, K. H. Freeman, Brian N. Popp, and C. H. Hoham. Compound-specific isotope analyses: A novel tool for reconstruction of ancient biogeochemical processes. *Organic Geochemistry*, 16:1115–1128, 1990.
- [14] J. M. Hayes, B. N. Popp, R. Takigiku, and M. W. Johnson. An isotopic study of biogeochemical relationships between carbonates and organic carbon in the Greenhorn Formation. *Geochimica and Cosmochimica Acta*, 53:2961–2972, 1989.
- [15] J. M. Hayes, H. Strauss, and A. J. Kaufman. The abundance of ^{13}C in marine organic matter and isotopic fractionation in the global biogeochemical cycle of carbon during the past 800 Ma. *Chemical Geology*, 161:103–125, 1999.

- [16] S. P. Hesselbo, D. R. Gröcke, H. C. Jenkyns, C. J. Bjerrum, P. Farrimond, H. S. M. Bell, and O. R. Green. Massive dissociation of gas hydrate during a Jurassic oceanic anoxic event. *Nature*, 406:392–395, 2000.
- [17] J. P. Jasper and R. B. Gagosian. The sources and deposition of organic matter in the Late Quaternary Pigmy Basin, Gulf of Mexico. *Geochimica et Cosmochimica Acta*, 54:1117–32, 1990.
- [18] H. C. Jenkyns. The early Toarcian (Jurassic) anoxic event: stratigraphic, sedimentary and geochemical evidence. *American Journal of Science*, 288:101–151, 1988.
- [19] H. C. Jenkyns and C. J. Clayton. Black shales and carbon isotopes in pelagic sediments from the Tethyan Lower Jurassic. *Sedimentology*, 33:87–106, 1986.
- [20] H. C. Jenkyns and C. J. Clayton. Lower Jurassic epicontinental carbonates and mudstones from England and Wales: chemostratigraphic signals and the early Toarcian anoxic event. *Sedimentology*, 44:687–706, 1997.
- [21] H. C. Jenkyns, D. R. Gröcke, and S. P. Hesselbo. Nitrogen isotope evidence for water mass denitrification during the early Toarcian (Jurassic) ocean anoxic event. *Paleoceanography*, 16:593–603, 2001.
- [22] A. P. Jimenez, C. Jimenez de Cisneros, P. Rivas, and J. A. Vera. The early Toarcian anoxic event in the westernmost Tethys (Subbetic): Paleogeographic and paleobiogeographic significance. *The Journal of Geology*, 104:399–416, 1996.
- [23] M. P. Koopmans, J. Köster, H. M. E. van Kaam-Peters, F. Kenig, S. Schouten, W. A. Hartgers, J. W. de Leeuw, and J. S. Sinninghe Damsté. Diagenetic and catagenetic products of isorenieratene: Molecular indicators for photic zone anoxia. *Geochimica et Cosmochimica Acta*, 60:4467–4496, 1996.
- [24] W. Küspert. Environmental changes during oil shale deposition as deduced from stable isotope ratios. In G. Einsele and A. Seilacher, editors, *Cyclic and event stratification*, pages 482–501. Springer-Verlag, New York, 1982.

- [25] C. T. S. Little and M. J. Benton. Early Jurassic mass extinction: A global long-term event. *Geology*, 23:495–498, 1995.
- [26] G. A. Logan, J. M. Hayes, G. B. Hieshima, and R. E. Summons. Terminal Proterozoic reorganization of biogeochemical cycles. *Nature*, 376:53–536, 1995.
- [27] G. A. Logan, R. E. Summons, and J. M. Hayes. An isotopic biogeochemical study of the Neoproterozoic and early Cambrian sediments from the Centralian Superbasin, Australia. *Geochimica and Cosmochimica Acta*, 61:5391–5409, 1997.
- [28] J. M. McArthur, D. T. Donovan, M. F. Thirlwall, B. W. Fouke, and D. Matthey. Strontium isotope profile of the early Toarcian (Jurassic) oceanic anoxic event, the duration of ammonite biozones and belemnite palaeotemperatures. *Earth and Planetary Science Letters*, 179:269–285, 2000.
- [29] J. C. McElwain, J. Wade-Murphy, and S. P. Hesselbo. Changes in carbon dioxide during an oceanic anoxic event linked to intrusion into gondwana coals. *Nature*, 435:479–482, 2005.
- [30] K. D. Monson and J. M. Hayes. Carbon isotope fractionation in the synthesis of bacterial fatty acids. Ozonolysis of unsaturated fatty acids as a means of determining the intramolecular distribution of carbon isotopes. *Geochimica et Cosmochimica Acta*, 46:139–149, 1982.
- [31] A. P. Murray, D. Edwards, J. M. Hope, C. J. Boreham, W. E. Booth, R. A. Alexander, and R. E. Summons. Carbon isotope biogeochemistry of plant resins and derived hydrocarbons. *Organic Geochemistry*, 29:1199–1214, 1998.
- [32] J. Palfy and P. L. Smith. Synchrony between Early Jurassic extinction, oceanic anoxic event and the Karoo Ferrar flood basalt volcanism. *Geology*, 8:747–750, 2000.
- [33] R. D. Pancost and C. S. Boot. The palaeoclimatic utility of terrestrial biomarkers in marine sediments. *Marine Chemistry*, 92:239–261, 2004.

- [34] K. E. Peters, C. C. Walters, and J. M. Moldowan. *The Biomarker Guide, Volume 1: Biomarkers and Isotopes in the Environment and Human History*. Cambridge University Press, Cambridge, UK, 2005.
- [35] K. E. Peters, C. C. Walters, and J. M. Moldowan. *The Biomarker Guide, Volume 2: Biomarkers and Isotopes in Petroleum Exploration and Earth History*. Cambridge University Press, Cambridge, UK, 2005.
- [36] H-J. Röhl, A. Schmid-Röhl, W. Oschmann, A. Frimmel, and L. Schwark. The Posidonia shale (Lower Toarcian) of SW-Germany: an oxygen-depleted ecosystem controlled by sea level and palaeoclimate. *Palaeogeography, Palaeoclimatology, Palaeoecology*, 169:273–299, 2001.
- [37] I. Rosales, S. Robles, and S. Quesada. Primary and diagenetic isotopic signals in fossils and hemipelagic carbonates: the Lower Jurassic of northern Spain. *Sedimentology*, 48:1149–1169, 2001.
- [38] I. Rosales, S. Robles, and S. Quesada. Elemental and oxygen isotope composition of early Jurassic belemnites: Salinity vs. temperature signals. *Journal of Sedimentary Research*, 74:342–354, 2004.
- [39] G. Sælen, P. Doyle, and M. R. Talbot. Stable-isotope analyses of belemnite rostra from the Whitby Mudstone Fm., England: surface water conditions during deposition of a marine black shale. *Palaios*, 11:97–117, 1996.
- [40] G. Sælen, R. V. Tyson, N. Telnæs, and M. R. Talbot. Contrasting watermass conditions during deposition of the Whitby Mudstone (Lower Jurassic) and Kimmeridge Clay (Upper Jurassic) formations, UK. *Palaeogeography, Palaeoclimatology, Palaeoecology*, 163:163–196, 2000.
- [41] J.L. Sarmiento, T.D. Herbert, and J.R. Toggweiler. Causes of anoxia in the world ocean. *Global Biogeochemical Cycles*, 2:115–128, 1988.
- [42] S. O. Schlanger and H. C. Jenkyns. Cretaceous ocean anoxic events: Causes and consequences. *Geologie en Mijnbouw*, 55:179–184, 1976.

- [43] S. S. Schouten, H. M. E. van Kaam-Peters, W. I. C. Rijpstra, M. Schoell, and J. S. Sinninghe-Damsté. Effects of an oceanic anoxic event on the stable carbon isotopic composition of early Toarcian carbon. *American Journal of Science*, 300:1–22, 2000.
- [44] H. Strauss and W. Peters-Kottig. The Paleozoic to Mesozoic carbon cycle revisited: the carbon isotopic composition of terrestrial organic matter. *Geochemistry, Geophysics, Geosystems*, 4:1083, doi:10.1029/2003GC000555, 2003.
- [45] R. E. Summons, L. L. Jahnke, J. M. Hope, and G. A. Logan. 2-Methylhopanoids as biomarkers for cyanobacterial oxygenic photosynthesis. *Nature*, 400:554–557, 1999.
- [46] R. E. Summons, J. K. Volkman, and C. J. Boreham. Dinosterane and other steroidal hydrocarbons of dinoflagellate origin in sediments and petroleum. *Geochimica et Cosmochimica Acta*, 51:3075–3082, 1987.
- [47] B. van de Schootbrugge, T. R. Bailey, Y. Rosenthal, M. E. Katz, J. D. Wright, K. G. Miller, S. Feist-Burkhardt, and P. G. Falkowski. Early Jurassic climate change and the radiation of organic-walled phytoplankton in the Tethys Ocean. *Paleobiology*, 31:73–97, 2005.
- [48] J. Veizer, D. Ala, K. Azmy, P. Bruckschen, D. Buhl, F. Bruhn, G. A. F. Carden, A. Diener, S. Ebner, Y. Godderis, T. Jasper, C. Korte, F. Pawellek, O. G. Podlaha, and H. Strauss. $^{87}\text{Sr}/^{86}\text{Sr}$, $\delta^{13}\text{C}$ and $\delta^{18}\text{O}$ evolution of Phanerozoic seawater. *Chemical Geology*, 161:59–88, 1999.
- [49] R. Zhang, M. J. Follows, J. P. Grotzinger, and J. Marshall. Could the late Permian deep ocean have been anoxic? *Paleoceanography*, 16:317–329, 2001.